A PKD-MFF signaling axis couples mitochondrial fission to mitotic progression

Evanthia Pangou, Olga Bielska, Lucile Guerber, Stephane Schmucker, Arantxa Agote-Arán, Taozhi Ye, Yongrong Liao, Marta Puig-Gamez, Erwan Grandgirard, Charlotte Kleiss, et al.

Cell Reports

Article

A PKD-MFF signaling axis couples mitochondrial fission to mitotic progression

Graphical abstract

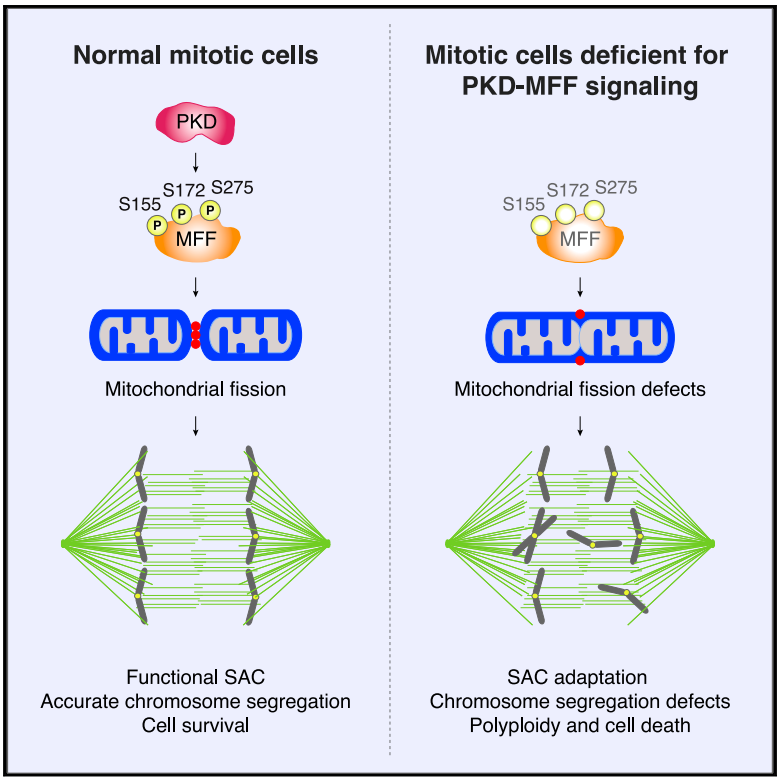

Authors

Evanthia Pangou, Olga Bielska, Lucile Guerber, ..., Ruedi Aebersold, Romeo Ricci, Izabela Sumara

Correspondence

ricci@igbmc.fr (R.R.), sumara@igbmc.fr (I.S.)

In brief

Pangou et al. show that PKD directly phosphorylates MFF specifically during mitosis to promote mitochondrial fission and proper chromosome segregation. PKD-dependent MFF phosphorylation inhibits adaptation of the mitotic checkpoint and provides a survival benefit to proliferating cells.

Highlights

- PKD and MFF drive mitotic mitochondrial fission and chromosome segregation
- PKD but not AMPK directly phosphorylates MFF specifically during mitosis
- PKD-phosphorylated MFF is required and sufficient for mitotic mitochondrial fission
- PKD-phosphorylated MFF protects cells from mitotic checkpoint slippage

Pangou et al., 2021, Cell Reports *35*, 109129
May 18, 2021
https://doi.org/10.1016/j.celrep.2021.109129

CellPress

Cell Reports

CellPress
OPEN ACCESS

Article

A PKD-MFF signaling axis couples mitochondrial fission to mitotic progression

Evanthia Pangou,[1,2,3,4,9] Olga Bielska,[1,2,3,4,9,10] Lucile Guerber,[1,2,3,4] Stephane Schmucker,[1,2,3,4] Arantxa Agote-Arán,[1,2,3,4] Taozhi Ye,[1,2,3,4] Yongrong Liao,[1,2,3,4] Marta Puig-Gamez,[1,2,3,4] Erwan Grandgirard,[1,2,3,4] Charlotte Kleiss,[1,2,3,4] Yansheng Liu,[5] Emmanuel Compe,[1,2,3,4] Zhirong Zhang,[1,2,3,4] Ruedi Aebersold,[6,7] Romeo Ricci,[1,2,3,4,8,*] and Izabela Sumara[1,2,3,4,11,*]

[1]Institut de Génétique et de Biologie Moléculaire et Cellulaire (IGBMC), Illkirch, France
[2]Centre National de la Recherche Scientifique UMR 7104, Strasbourg, France
[3]Institut National de la Santé et de la Recherche Médicale U964, Strasbourg, France
[4]Université de Strasbourg, Strasbourg, France
[5]Cancer Biology Institute, Yale School of Medicine, West Haven, CT, USA
[6]Institute of Molecular Systems Biology, Department of Biology, ETH Zürich, Zürich, Switzerland
[7]Faculty of Science, University of Zürich, Zürich, Switzerland
[8]Laboratoire de Biochimie et de Biologie Moléculaire, Nouvel Hôpital Civil, Strasbourg, France
[9]These authors contributed equally
[10]Present address: Buck Institute for Research on Aging, Novato, CA, USA
[11]Lead contact
*Correspondence: ricci@igbmc.fr (R.R.), sumara@igbmc.fr (I.S.)
https://doi.org/10.1016/j.celrep.2021.109129

SUMMARY

Mitochondria are highly dynamic organelles subjected to fission and fusion events. During mitosis, mitochondrial fission ensures equal distribution of mitochondria to daughter cells. If and how this process can actively drive mitotic progression remains largely unknown. Here, we discover a pathway linking mitochondrial fission to mitotic progression in mammalian cells. The mitochondrial fission factor (MFF), the main mitochondrial receptor for the Dynamin-related protein 1 (DRP1), is directly phosphorylated by Protein Kinase D (PKD) specifically during mitosis. PKD-dependent MFF phosphorylation is required and sufficient for mitochondrial fission in mitotic but not in interphasic cells. Phosphorylation of MFF is crucial for chromosome segregation and promotes cell survival by inhibiting adaptation of the mitotic checkpoint. Thus, PKD/MFF-dependent mitochondrial fission is critical for the maintenance of genome integrity during cell division.

INTRODUCTION

Mitochondria are vital organelles that are often described as the powerhouse of the cell. As such, they regulate critical cellular processes, including energy production, cellular metabolism, and apoptosis (Herst et al., 2017). Mitochondria are highly dynamic organelles, which constantly undergo events of fission (division), fusion, and cytoskeleton-based transport. Mitochondrial fission is mediated by recruitment of the GTPase Dynamin-related protein 1 (DRP1) at the mitochondrial outer membrane by the following specific mitochondrial receptors: mitochondrial fission factor (MFF) (Gandre-Babbe and van der Bliek, 2008), Fis1, MiD49, or MiD51 (Losón et al., 2013). Mitochondrial fusion is mediated by the mitofusins MFN1 and MFN2 and by GTPase optic atrophy 1 (OPA1) (Silva Ramos et al., 2019).

MFF is the predominant DRP1 receptor in mammalian cells (Otera et al., 2010) and is highly expressed in tissues with high energy demands, such as heart, brain, muscle, kidney, and liver (Gandre-Babbe and van der Bliek, 2008). Knockdown of MFF results in elongated mitochondria, whereas transient MFF overexpression causes increased mitochondrial fragmentation (Otera et al., 2013). Despite its fundamental importance for mitochondrial dynamics, the regulatory mechanisms upstream of MFF have only recently started to be investigated. In response to energy stress, MFF is phosphorylated by the AMP-activated protein kinase (AMPK) to recruit DRP1 to mitochondria and drive mitochondrial fragmentation (Toyama et al., 2016). Under non-stress conditions, MFF was also shown to be ubiquitylated by the Parkin ligase that triggers its lysosomal degradation (Lee et al., 2019).

In addition to cellular stress responses, mitochondrial dynamics is also tightly regulated during cell cycle progression. In interphase cells, mitochondria form tubular networks, which are fragmented during mitosis, thereby facilitating their equal distribution to daughter cells (Kanfer and Kornmann, 2016). Mitotic phosphorylation of DRP1 by CDK1 drives fragmentation of the mitochondrial network starting in late prophase (Taguchi et al., 2007). In addition, synergistic action of Aurora A and CDK1 kinases promote DRP1 phosphorylation through the Ras-like GTPase RalA and its effector RalBP1 (Kashatus et al., 2011) to regulate mitochondrial fission during mitosis. However, given that a high energy demand is required to fuel the mitotic

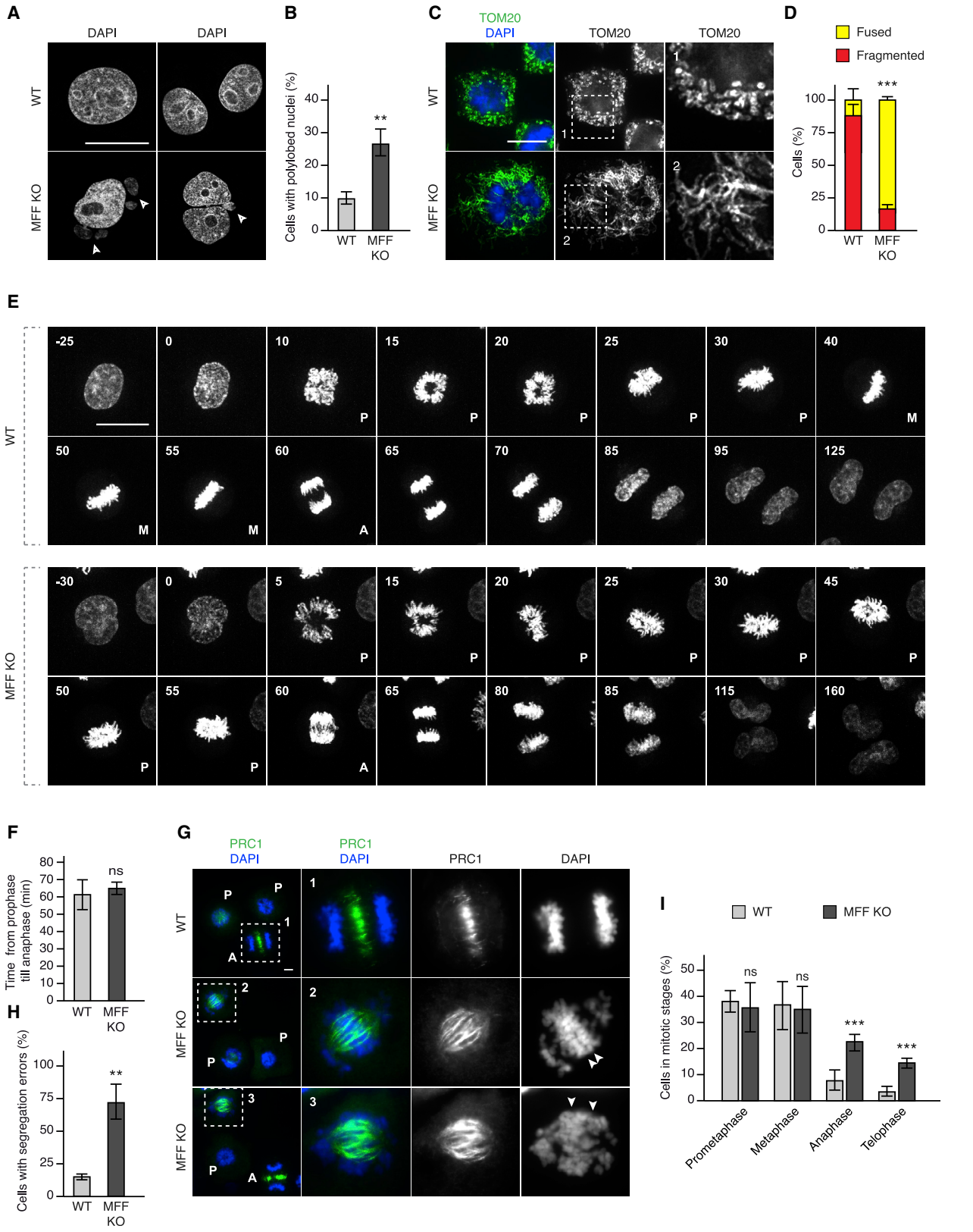

(legend on next page)

cycle (Salazar-Roa and Malumbres, 2017), it remains elusive whether and how additional molecular events might actively link the mitochondrial fission machinery to the regulation of mitotic progression.

Here, we demonstrate that MFF is directly phosphorylated by the high-energy-sensing kinase Protein Kinase D (PKD) specifically during mitosis and independently of AMPK. Lack of PKD-dependent MFF phosphorylation alleviates mitochondrial fragmentation during mitosis but not in interphase. Importantly, PKD-dependent MFF phosphorylation is crucial for chromosome segregation and promotes cell survival by inhibiting adaptation of the mitotic checkpoint. Our results thus reveal an unexpected role for PKD signaling in mitosis coupling mitochondrial fission to mitotic progression, which may provide a survival benefit to proliferating cells.

RESULTS

MFF drives mitotic mitochondrial fission and is required for proper chromosome segregation

To address the requirement of MFF in mitosis, we first downregulated MFF, the mitochondrial fusion factor OPA1 as a negative control (Cipolat et al., 2004; Park and Cho, 2012), and DRP1 as a positive control (Díaz-Martínez et al., 2014; Peña-Blanco et al., 2020) by using specific small interfering RNAs (siRNAs) in HeLa cells (Figures S1A and S1B). As expected DRP1- and MFF-depleted cells displayed fused and elongated mitochondria relative to cells treated with control siRNA where mitochondria were tubular, whereas OPA1 depletion led to a more fragmented mitochondrial phenotype (Figure S1C). Interestingly, DRP1- and MFF- but not OPA1-depleted cells displayed polylobed nuclei and an increase in 4N DNA content (Figures S1C–S1E) relative to cells treated with control siRNA.

Deletion of all MFF isoforms in HeLa cells by using CRISPR-Cas9-mediated gene editing (Figures S1F and S1G) confirmed the polylobed nuclei phenotype (Figures 1A and 1B), as well as the increased 4N DNA content relative to isogenic wild-type (WT) cells (Figure S1H). Moreover, during mitosis, MFF knockout (KO) cells showed a fused mitochondrial network (Figures 1C and 1D), in contrast to fragmented mitochondria in WT mitotic cells. These findings suggest that in addition to its role during interphase, MFF is also required for mitochondrial fission during mitosis.

Time-lapse video microscopy revealed that mitotic entry and timing of mitotic progression from prophase until anaphase was not affected by deletion of MFF, but MFF KO cells frequently proceeded to anaphase before all chromosomes were properly aligned or directly from a prolonged prometaphase stage (Figures 1E and 1F). MFF KO cells displayed segregation errors and frequently exited mitosis with polylobed nuclei (Figures 1E, 1G, 1H, and S2A). The fact that MFF-depleted cells exited mitosis in a timely manner similar to their parental WT cells despite segregation errors was unexpected and raised more questions regarding their mitotic status. Interestingly, the midzone formation factor protein regulator of cytokinesis 1 (PRC1) (Mollinari et al., 2002) localized to robust microtubule bundles in MFF KO cells that displayed chromosomal abnormalities including misalignment and aberrant segregation (Figures 1G and 1H), suggesting that anaphase-like sister chromatid movements took place before misaligned chromosomes were repositioned to the metaphase plate (Figure 1G). Additionally, MFF KO cells displayed an increased number of cells in anaphase and telophase stages (Figure 1I) relative to WT control as well as chromosome alignment and segregation defects including lagging chromosomes and chromosomal bridges and, as expected, a fused mitochondrial network throughout mitosis (Figure S2A). Similarly, U2OS cells treated with specific siRNAs against MFF (Figure S2B) displayed segregation errors and fused mitochondria during cell division relative to cells treated with control siRNA (Figures S2C–S2E). Our results suggest that MFF is required for fragmentation of mitochondria and for chromosome segregation during mitosis and that MFF deficiency may lead to nuclear abnormalities and compromise genome integrity in mammalian cells.

Given that DRP1 has already been linked to faithful cell division (Yamano and Youle, 2011), we next asked if other DRP1 mitochondrial receptors, in addition to MFF, are involved in mitotic progression. To this end, we used specific siRNAs against MID49 (Figures S3A and S3B). As expected, DRP1 depletion yielded segregation errors of similar severity as the ones in MFF-depleted mitotic cells. In contrast, depletion of MID49 did not result in segregation errors relative to control-depleted cells (Figures S3B and S3C). Thus, MFF rather exerts non-redundant functions in mitosis.

We next tested the possibility that the chromosome segregation phenotype of MFF-depleted cells could be rescued by

Figure 1. MFF drives mitotic mitochondrial fission and chromosome segregation

(A and B) Immunofluorescence (IF) of WT and MFF KO HeLa cells synchronized with double thymidine block and release (DTBR) in G1. Arrowheads point to nuclear regions of irregular shape. Nuclei were stained with 4′,6-diamidino-2-phenylindole (DAPI). Scale bar, 5 μm. The percentage of cells with abnormal nuclei was quantified in (B). At least 300 cells per condition were analyzed (mean ± SD, **$p < 0.01$, two-tailed t test, n = 3).

(C and D) IF of WT and MFF KO HeLa cells synchronized with DTBR in mitosis. Regions of interest (ROIs) are shown in the corresponding numbered panels. TOM20 was used as a mitochondrial marker, and chromosomes were stained with DAPI. Scale bar, 5 μm. The percentage of cells with fragmented or fused mitochondrial morphology was quantified in (D). At least 300 cells per condition were analyzed (mean ± SD, ***$p < 0.001$, two-tailed t test, n = 3).

(E and F) Spinning disk time lapse microscopy of WT and MFF KO HeLa cells synchronized with DTBR in mitosis. The selected frames of the movies are depicted and time is shown in min. P, M, and A refer to images corresponding to prometaphase, metaphase, and anaphase, respectively. SiR-DNA was used to stain DNA. Scale bar, 5 μm. The average time (min) from prophase to anaphase was quantified in (F). At least 70 cells per condition were analyzed (mean ± SD, ns = non-significant, two-tailed t test, n = 3).

(G–I) IF of WT and MFF KO HeLa cells synchronized for 16 h with monastrol in mitosis and collected 90 min after release from monastrol. ROIs are shown in the corresponding numbered panels. PRC1 was used as a mitotic spindle marker, and chromosomes were stained with DAPI. Arrowheads point to chromosome segregation errors. Scale bar, 5 μm. The percentage of cells displaying segregation errors was quantified in (H), and the percentage of cells as distributed in different mitotic stages was quantified in (I). At least 300 cells per condition were analyzed (mean ± SD, ***$p < 0.001$, **$p < 0.01$, two-tailed t test, n = 3).

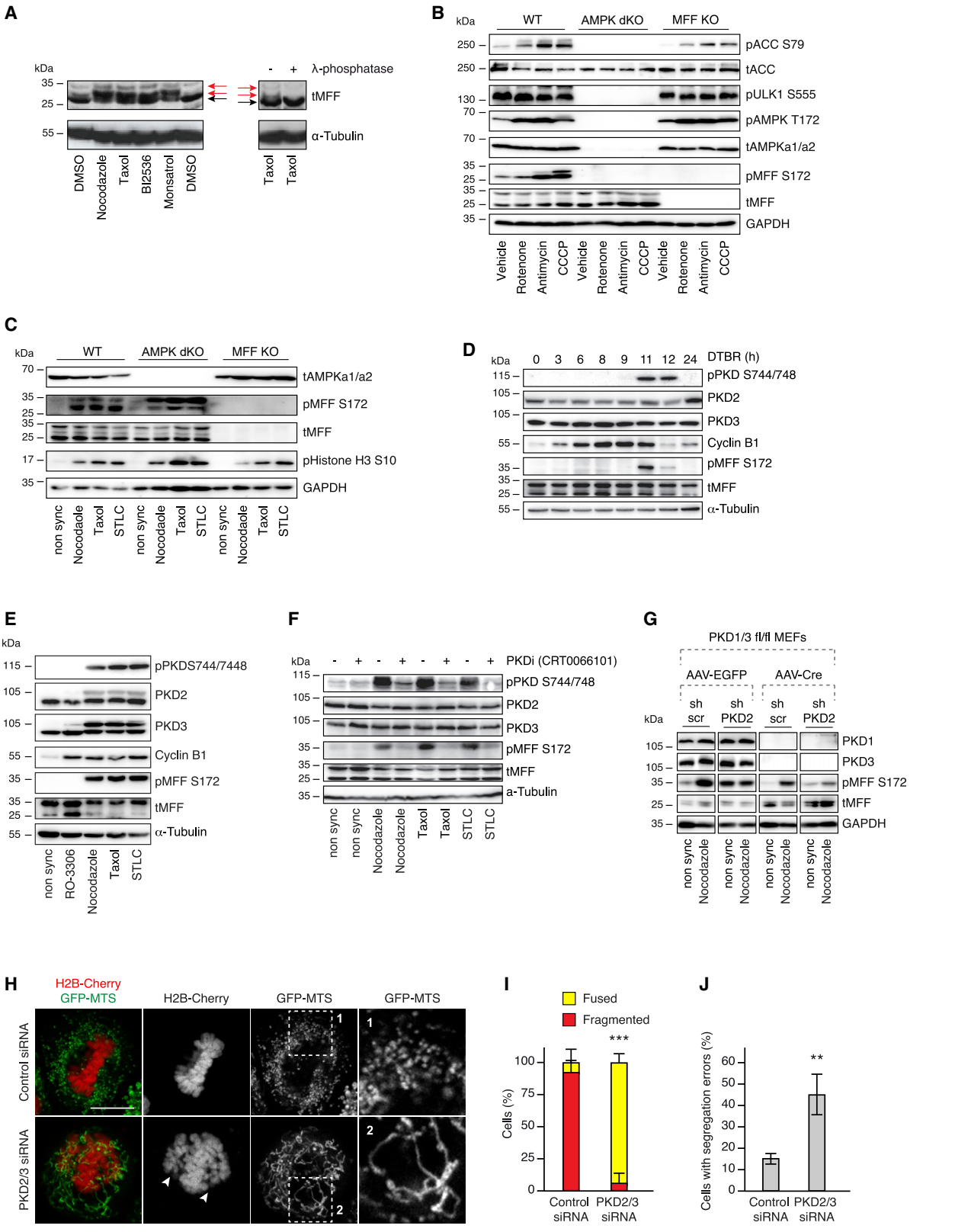

(legend on next page)

disabling the fusion machinery, as it has been demonstrated for cardiac-failure-induced lethality in MFF KO mice (Chen et al., 2015). MFF KO and parental WT cells were treated with specific siRNAs against fusion factor MFN1 (Figure S3D). MFN1 silencing did not lead to chromosome segregation errors in WT cells, but it fully rescued this phenotype in MFF-deficient cells (Figures S3E and S3F). Thus, fusion deficiency can counterbalance the mitotic defects in MFF-deficient cells, supporting a potential link between MFF-dependent mitochondrial fission and proper mitotic progression.

MFF phosphorylation during mitosis depends on PKD kinase activity

Recently, MFF was discovered to be phosphorylated by AMPK kinase to recruit DRP1 and to drive mitochondrial fragmentation in response to energy stress (Toyama et al., 2016). To explore the possibility that MFF may be subjected to posttranslational regulation during mitosis, we compared non-synchronized, solvent-treated HeLa cells with cells arrested in mitosis by treatment with the microtubule poisons nocodazole or taxol, the polo-like kinase 1 (PLK1) inhibitor BI2536, or the kinesin Eg5 inhibitor monastrol (Figure 2A). This analysis revealed a shift in the electrophoretic mobility of MFF in mitotic extracts, which was abolished by treatment with alkaline phosphatase (Figure 2A), suggesting that MFF is phosphorylated during mitosis. To test if AMPK is responsible for MFF phosphorylation during mitotic division, we generated HEK293T cells that lack both catalytic subunits of AMPK (AMPKα1/α2 double KO [dKO]) by using CRISPR-Cas9 gene editing as described previously (Toyama et al., 2016). AMPK dKO cells showed no AMPK activity in response to different established activators monitored by AMPK-phospho-substrate antibodies (pACC S79 and pULK1 S555) (Figure 2B). In line with the previous report (Toyama et al., 2016), AMPK dKO cells displayed significantly reduced MFF phosphorylation on Ser172, an effect particularly striking upon treatment with the mitochondrial poisons rotenone, antimycin, or carbonyl cyanide 3-chlorophenylhydrazone (CCCP) (Figure 2B). Strikingly, in contrast to energy stress conditions, mitotic phosphorylation of MFF at Ser172 was fully retained in the absence of AMPK (Figure 2C), indicating that AMPK activity is not required for mitotic MFF phosphorylation. Interestingly, mitotic MFF phosphorylation in AMPK dKO cells appeared to be increased relative to control cells, which could be due to the absence of negative regulation of PKD1 by AMPK, as reported previously in the context of the insulin pathway in C2C12 skeletal muscle cells (Coughlan et al., 2016).

A previously reported, proteomic analysis identified MFF phosphorylation on Ser155 and Ser172 in HEK293T cells upon nocodazole treatment and overexpression of protein kinase D1 (PKD1) (Britton et al., 2014). PKD1 is the founder kinase of the PKD Ser/Thr kinase family and is highly homologous to the other two members, namely, PKD2 and PKD3. PKDs have been previously described to regulate formation of transport carriers from the *trans*-Golgi network (TGN) as well as actin polymerization (Franz-Wachtel et al., 2012; Gehart et al., 2012; Malhotra and Campelo, 2011). Analysis of PKD activatory phosphorylation on Ser744/748 (Eiseler et al., 2010) in HeLa cells synchronized in different cell cycle stages revealed a strong induction of phosphorylation on these PKD residues specifically during mitosis, before onset of Cyclin B degradation, which correlated with MFF phosphorylation at Ser172 (Figure 2D). Analysis of PKD activatory phosphorylation on Ser744/748 (Eiseler et al., 2010) in HeLa cells synchronized in different cell cycle stages revealed strong PKD activity specifically during mitosis, before the onset of Cyclin B degradation, which correlated with MFF phosphorylation at Ser172 (Figure 2D). PKD2 and PKD3 expression was largely unaffected during cell cycle progression (Figure 2D), whereas PKD1 is not expressed in HeLa cells (Yeaman et al., 2004). These phosphorylation events were also observed in mitotic cells synchronized by nocodazole, taxol, or the Eg5 inhibitor STLC but not in G2-arrested cells induced by the CDK1 inhibitor RO-3306 or in non-synchronized interphasic cells (Figure 2E). PKD inhibition using CRT0066101 (Yuan et al., 2006) largely abolished mitotic MFF Ser172 phosphorylation in HeLa cells (Figure 2F). Likewise, mouse embryonic fibroblasts (MEFs) lacking all three PKD kinases displayed strong reduction in mitotic MFF phosphorylation (Figure 2G), although some remaining Ser172 phosphorylation signal could be detected, likely due to residual PKD2 activity following its downregulation by short hairpin RNA (shRNA) treatment in PKD1/3-deleted MEFs (Figure S4A). These results suggest that PKD, but not AMPK, is required for MFF phosphorylation during mitosis.

Figure 2. MFF phosphorylation during mitosis depends on PKD kinase activity

(A) Western blot (WB) of unsynchronized or mitotically arrested WT HeLa cells by using nocodazole, taxol, BI2536, or monastrol in the absence and presence of λ phosphatase. The black arrow indicates non-modified MFF protein (tMFF, total MFF), whereas the two red arrows indicate up-shifted MFF.

(B) WB of unsynchronized WT, AMPK α1/α2 double knockout (AMPK dKO), and MFF knockout (MFF KO) HEK293T cells treated with rotenone, antimycin, CCCP, or vehicle.

(C) WB of WT, AMPK dKO, and MFF KO HEK293T cells unsynchronized or mitotically arrested using nocodazole, taxol, or STLC.

(D) WB of WT HeLa cells synchronized with DTBR. Time points in h correspond to different cell cycle stages.

(E) WB of unsynchronized WT HeLa cells, or arrested in G2 (RO-3306) or mitotically arrested as in (C).

(F) WB of WT HeLa cells mitotically arrested as in (C) in the absence and presence of the PKD inhibitor (CRT0066101).

(G) WB of mouse embryonic fibroblasts (MEFs) derived from PKD1/3 double-floxed mice infected either with adeno-associated virus (AAV) containing EGFP (AAV-EGFP) or Cre recombinase (AAV-Cre) and co-expressing either a scrambled or a PKD2-targeting shRNA. Cells were unsynchonized or mitotically arrested using nocodazole.

(H–J) Fluorescence of WT HeLa cells stably expressing H2B-mCherry and a GFP-tagged mitochondrial-targeting sequence (GFP-MTS) treated with the indicated siRNAs, synchronized for 16 h with monastrol in mitosis, and collected 90 min after release from monastrol. ROIs are shown in the corresponding numbered panels. Arrowheads point to chromosome segregation errors. Scale bar, 5 μm. The percentage of cells with fragmented or fused mitochondrial morphology was quantified in (I), and the percentage of cells displaying segregation errors was quantified in (J). At least 300 cells per condition were analyzed (mean ± SD, ***$p < 0.001$, **$p < 0.01$, two-tailed t test, $n = 3$).

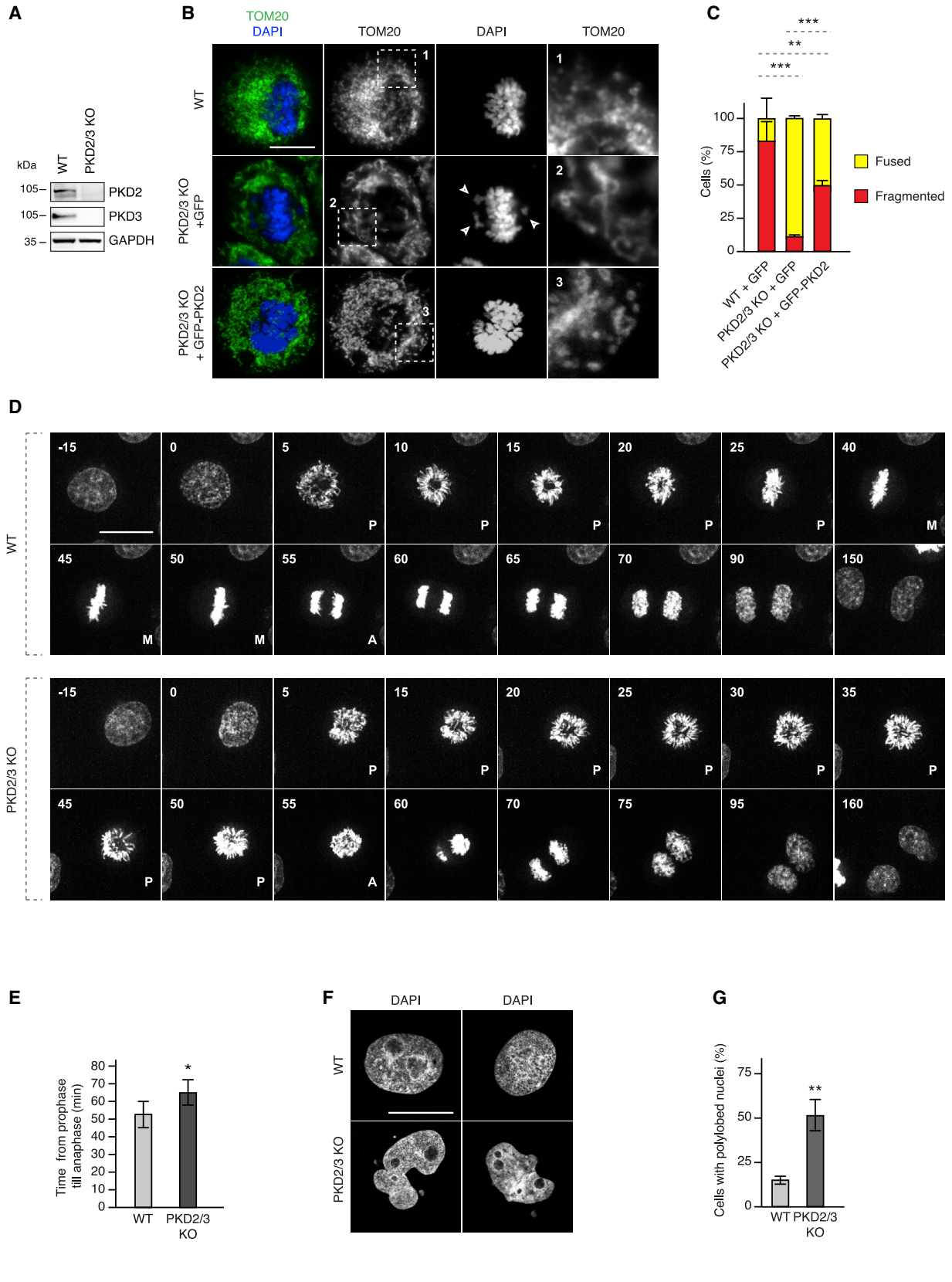

(legend on next page)

PKD is required for mitotic mitochondrial fission and for chromosome segregation

To understand the physiological relevance of PKD-mediated MFF phosphorylation during mitosis, we first silenced both PKD2 and PKD3 (Figure S4B) in HeLa cells stably expressing H2B-mCherry and a GFP-tagged mitochondrial-targeting sequence (GFP-MTS) (Figure S4B). PKD2/PKD3-downregulated cells displayed fused and elongated mitochondria during mitotic progression relative to control cells (Figures 2H, 2I, and S4C). Strikingly, PKD2/PKD3-downregulated cells displayed mitotic defects highly similar to MFF-deficient cells, with premature anaphase-like phenotype and segregation errors (Figures 2H, 2J, and S4C). These results were further verified in HeLa cells deleted for PKD2 and PKD3 (PKD2/3 dKO) by using CRISPR-Cas9 gene editing (Figures 3A and S4D). As expected, PKD2/3 dKO cells displayed fused and elongated mitochondria relative to parental WT cells, although mitochondrial elongation in PKD2/3 dKO cells appeared to be milder than in PKD2/3 siRNA cells, likely due to a genetic compensation. Nevertheless, this phenotype could be partially rescued by overexpression of the GFP-tagged PKD2 (Figures 3B and 3C). Because a previous study reported a role for PKD in mitochondrial fragmentation in cardiomyocytes (Jhun et al., 2018), we asked if PKD represents a general mitochondrial fission regulator and tested whether PKD deficiency might impair mitochondrial fission during interphase. The mitochondria of unsynchronized PKD2/3 dKO cells were characterized as partially fragmented or tubular, and this morphology was very similar to their corresponding parental WT cells (Figures S4E–SG). These observations suggest that PKD acts as an important MFF specifically during mitosis but not in interphase.

Highly reminiscent of phenotypes in MFF KO cells, PKD2/3 dKO cells displayed aberrant anaphase entry from a prolonged prometaphase-like stage, chromosome segregation errors (Figure 3D), and polylobed nuclei (Figures 3F and 3G). Contrary to MFF KO cells, the timing from prophase to anaphase was significantly increased in PKD2/3 KO cells, displaying a delay of around 10 min compared to control parental WT cells (Figures 3D and 3E), which could be explained by the accumulating evidence that PKDs have additional roles in mitosis (Papazyan et al., 2008; Roy et al., 2018). Taken together, our data suggest that PKD-dependent regulation of MFF promotes mitochondrial fission and proper mitotic progression in human cells.

PKD directly phosphorylates MFF on serines 155, 172, and 275

We next asked whether PKD directly phosphorylated MFF. To address this question, we first examined the interaction of PKD with MFF. Immunoprecipitations of FLAG-tagged MFF (FLAG-MFF) with GFP-tagged WT PKD1 (GFP-PKD1) cells revealed that both proteins can interact relative to a GFP-empty control (Figure 4A). Interestingly, the interaction of PKD with MFF increased in nocodazole-arrested mitotic cells relative to cells in G2 and in interphase stage (Figure 4A). To address if the MFF interaction with PKD can induce MFF phosphorylation, we immunoprecipitated FLAG-MFF co-expressed with WT, constitutively active (CA), or kinase-dead (KD) GFP-PKD1 in HEK293T cells and analyzed immunoprecipitates with a PKD phosphorylation consensus motif (LXRXXS/T) antibody (Döppler et al., 2005). Expression of CA-PKD potentiated phosphorylation of MFF relative to WT-PKD and KD-PKD and to control conditions in which basal MFF phosphorylation was detected most likely due to the presence of endogenous PKD kinases in HEK293T cells (Figure 4B).

Next, we subjected recombinant human MFF to a radioactive *in vitro* kinase assay by using recombinant PKD1-GST kinase. Autoradiography analysis revealed MFF phosphorylation and PKD autophosphorylation. Both signals were abolished in the presence of the PKD inhibitor (Figure 4C). Thus, PKD activity is required for MFF phosphorylation in human cells and is sufficient for this posttranslational modification *in vitro*.

To identify PKD phosphorylation sites on MFF, the *in vitro* kinase assay was scaled up 10-fold (Figure 4D) and analyzed by mass spectrometry (Figure S5A). This analysis combined with the results of the reported PKD substrate phosphoproteome (Franz-Wachtel et al., 2012) identified six candidate phosphorylation sites (Y39, T112, S155, S172, S275, and T280). Site-specific mutagenesis of recombinant MFF and *in vitro* kinase assay analysis confirmed Ser155, Ser172, and Ser275 as putative PKD phosphorylation sites by using both autoradiography (Figures 4E, S5B, and S5C) and phospho-specific antibodies (Figure 4F), whereby mutagenesis of all three sites was necessary to completely abolish the PKD-dependent phosphorylation signal on MFF (Figures 4E and 4H). Although Ser275 phosphorylation could be clearly detected in the mass spectrometry analysis (Figure S5A), its contribution seems to be minor compared to Ser155 and Ser172 at least *in vitro* (Figure 4E).

The three MFF phosphorylation sites are highly conserved across multiple MFF isoforms generated through alternative splicing and across vertebrate species (Figure 4G). To validate these sites in cells, we co-expressed WT and non-phosphorylatable (Ser to Ala) FLAG-MFF mutants together with GFP or GFP-PKD1-CA in HEK293T cells. Expression of GFP-PKD1-CA potentiated phosphorylation of all three sites in the presence (Figure 4H) and absence of AMPK (Figure S5D). Hence, we conclude that PKD directly phosphorylates Ser155, Ser172, and Ser275 on MFF.

Figure 3. PKD is required for mitotic mitochondrial fission and for chromosome segregation

(A) WB validation of CRISPR-Cas9-mediated dKO PKD2 and PKD3 (PKD2/3 dKO) HeLa cells.

(B and C) IF of WT and PKD2/3 dKO HeLa cells transfected with GFP-PKD2 or GFP alone, synchronized for 16 h with monastrol in mitosis, and collected 90 min after release from monastrol. ROIs are shown in the corresponding numbered panels. TOM20 was used as a mitochondrial marker, and chromosomes were stained with DAPI. Arrowheads point to misaligned chromosomes. Scale bar, 5 μm. The percentage of cells with fragmented or fused mitochondrial morphology was quantified in (C). At least 150 cells per condition were analyzed (mean ± SD, ***$p < 0.001$, **$p < 0.01$, two-tailed t test, n = 3).

(D and E) Spinning disk time lapse microscopy of WT and PKD2/3 dKO KO HeLa cells synchronized with DTBR in mitosis. The selected frames of the movies are depicted, and time is shown in min. SiR-DNA was used to stain DNA. Scale bar, 5 μm. The average time (min) from prophase to anaphase was quantified in (F). At least 70 cells per condition were analyzed (mean ± SD, *$p < 0.05$, two-tailed t test, n = 3).

(F and G) IF of WT and PKD2/3 dKO HeLa cells synchronized with DTBR in G1. Nuclei were stained with DAPI. Scale bar, 5 μm. The percentage of cells with polylobed nuclei was quantified in (G). At least 300 cells per condition were analyzed (mean ± SD, **$p < 0.01$, two-tailed t test, n = 3).

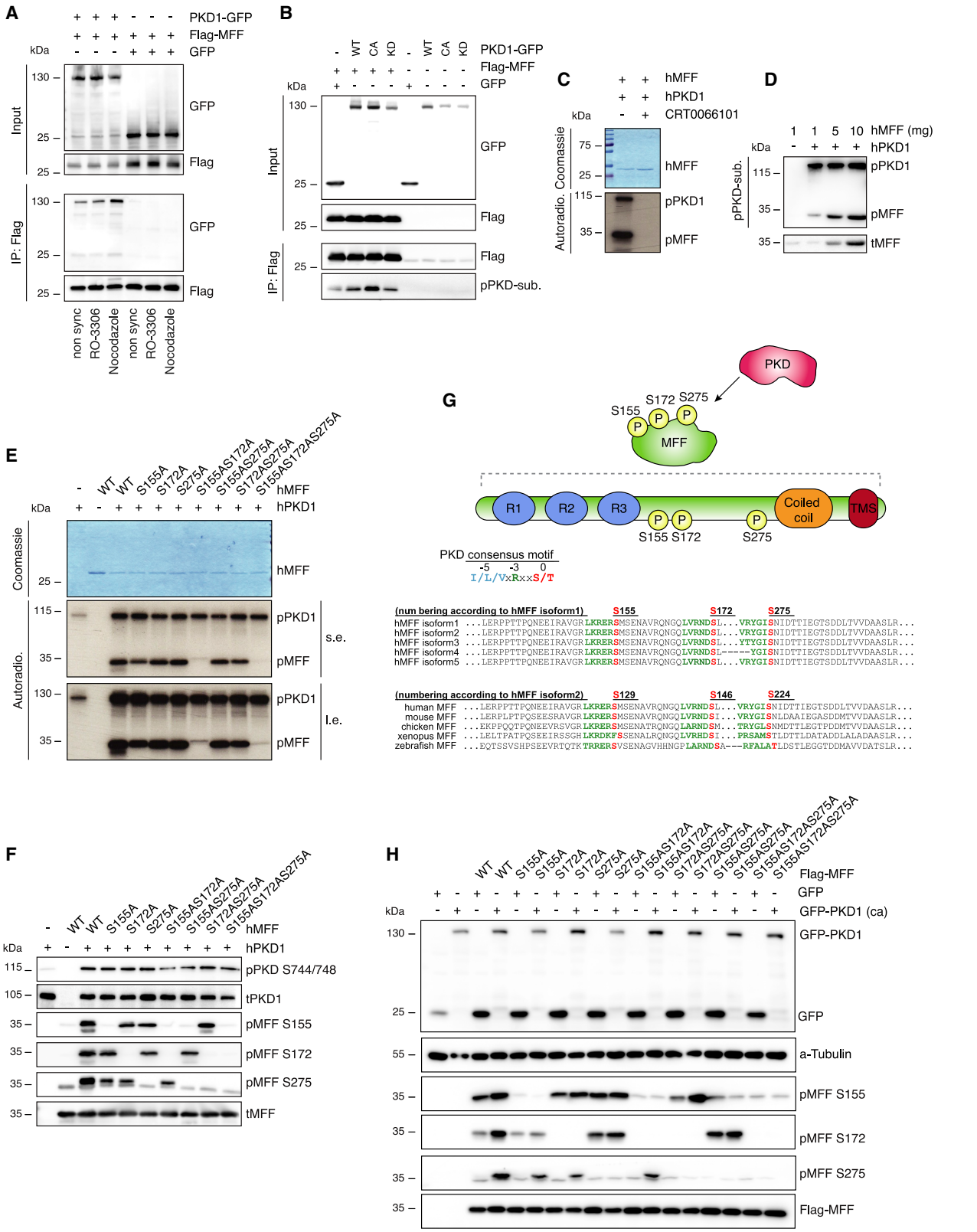

(legend on next page)

PKD-dependent MFF phosphorylation drives mitotic mitochondrial fission and promotes proper chromosome segregation

Having proven that MFF is a direct target of PKD, we next aimed to demonstrate that phosphorylation of MFF was important for mitotic mitochondrial fragmentation and progression through mitosis. Rescue experiments in MFF KO cells stably expressing WT or a non-phosphorylatable MFF 3SA (Figure 5A) revealed that in contrast to MFF 3SA, MFF WT efficiently restored mitochondria fragmentation in mitosis (Figures 5B and 5C). Thus, PKD-dependent phosphorylation of MFF is required for mitochondrial fission during mitosis.

Because the main function of MFF is to recruit DRP1 to the mitochondria (Otera et al., 2010), we wondered whether PKD-dependent phosphorylation of MFF affected the targeting of DRP1 to the outer mitochondrial membrane during mitosis. Mitochondrial recruitment of DRP1 was moderately but significantly reduced in cells depleted for MFF, and it could be restored in cells stably expressing MFF WT but not MFF 3SA, as indicated by co-localization with TOM20 (Figures S6A and S6B). We were unable to detect this slight reduction in DRP1 recruitment to the mitochondria by using biochemically purified mitochondria-containing cellular fractions (Figure S6C). Nevertheless, even a small reduction in mitochondrial DRP1 recruitment in cells deficient for MFF phosphorylation may affect the function (and possibly activation) of DRP1 and mitochondrial fission, for instance by regulating the relative levels of fission factors, as it has been demonstrated for the MID51/MID49-MFF-DRP1 triple complex (Yu et al., 2017).

Because MFF is generally required for mitochondrial fission, it was critical to verify that PKD-mediated MFF phosphorylation is specifically required for mitochondrial fission during mitosis but not in interphase, as it has been demonstrated above for PKD-deficient cells (Figures S4E–S4G). To this end, we performed the rescue experiments in interphase MFF KO cells stably expressing MFF WT or MFF 3SA. As expected, MFF depletion led to fused mitochondria in interphase, but in contrast to mitosis, this phenotype was fully restored irrespectively of the MFF phosphorylation status (Figures S6D and S6E), suggesting that PKD-mediated MFF phosphorylation drives mitotic but not interphase mitochondrial fission.

To further exclude a general mitochondria defect in cells deficient for MFF phosphorylation, we analyzed several metabolic parameters as a readout for the cellular fitness in different cell cycle stages in MFF KO cells and parental WT cells. We did not observe any differences in the mitochondrial membrane potential in any of the cell cycle stages (Figure S6F), which is a result in line with a recent study demonstrating that a lack of MFF activity does not impair mitochondria function in neuronal cells (Lewis et al., 2018). Interestingly, ATP production was strongly reduced in MFF KO cells compared to that of parental WT solely in mitotic but not in interphasic cells (Figure S6G). Thus, our results suggest that mitotic phenotypes in MFF-deficient cells are the direct consequence of lack of fission during mitosis, rather than the result of general mitochondrial defects.

Importantly, MFF KO cells stably expressing non-phosphorylatable MFF 3SA but not the MFF WT displayed chromosome segregation defects, including anaphase and telophase bridges (Figures 5C and 5D), which is highly similar to the phenotypes observed in MFF KO, MFF siRNA, PKD2/3 siRNA, and PKD2/3 dKO cells. Accordingly, the number of cells in anaphase and telophase stages, which was shown to be increased in MFF KO cells (Figure 1I), was also increased in cells expressing MFF 3SA, but not MFF WT, whereas prometaphase and metaphase stages were unaffected (Figures 5E–5H). Our results thus suggest that PKD-mediated MFF phosphorylation is required for the fidelity of chromosome segregation. The absence of this signaling may lead to the anaphase onset in the presence of improperly attached or unattached kinetochores as it is known, for instance, for cells deficient for the chromosomal passenger complex (CPC) (Vader et al., 2008).

To test if PKD-mediated MFF phosphorylation is required for chromosome bi-orientation at the mitotic spindle, we analyzed kinetochore localization of Astrin (SPAG5), a protein with an established role in promoting the stability of microtubule-kinetochore (MT-KT) attachments and faithful chromosome bi-orientation and segregation (Dunsch et al., 2011). The intensity of Astrin on individual kinetochores was moderately but significantly reduced in metaphase-synchronized MFF KO cells and in MFF KO cells expressing the non-phosphorylatable MFF 3SA relative to WT cells or MFF KO cells expressing MFF WT (Figures 5I and 5J). Thus, PKD-dependent MFF phosphorylation might be important to fine-tune the stability of MT-KT attachments during mitosis.

PKD-dependent MFF phosphorylation protects cells from SAC adaptation

MT-KT attachment defects potentiate activity of the spindle assembly checkpoint (SAC) (also known as the mitotic checkpoint), a safeguard mechanism triggering mitotic arrest to provide the

Figure 4. PKD directly phosphorylates MFF on serines 155, 172, and 275

(A) WB of immunoprecipitation of FLAG-MFF with GFP-PKD1 from HEK293T cells unsynchronized, arrested in G2 (RO-3306), or in mitosis (nocodazole).

(B) WB of immunoprecipitations of FLAG-MFF expressing WT, constitutively active (CA), kinase-dead (KD) GFP-PKD1, or GFP alone in HEK293T cells.

(C) Autoradiography and Coomassie staining of *in vitro* kinase assay with recombinant human MFF (hMFF) and recombinant human PKD1 (hPKD1) in the absence and presence of the PKD inhibitor CRT0066101.

(D) WB of reactions obtained in an *in vitro* kinase assay with hMFF in the absence or presence of hPKD1 by using PKD phospho-motif antibody (pPKD sub.).

(E) Autoradiography and Coomassie staining of *in vitro* kinase assay with WT and mutated hMFF in absence and presence of hPKD1. Short exposures (s.e.) and long exposures (l.e.) are shown.

(F) WB of reactions obtained in an *in vitro* kinase assay with WT and mutated hMFF in the absence and presence of hPKD1 by using MFF phospho-specific antibodies against phosphorylated Ser155, Ser172, and Ser275 on MFF and against phosphorylated active PKD (S744/748).

(G) Schematic view of PKD-dependent MFF phosphorylation sites and MFF protein domain organization. All three phosphorylation sites correspond to the PKD consensus phosphorylation motif and are conserved among human MFF isoforms and different species.

(H) WB of HEK293T cells co-expressing GFP-PKD1 CA or GFP alone with WT or mutated FLAG-MFF.

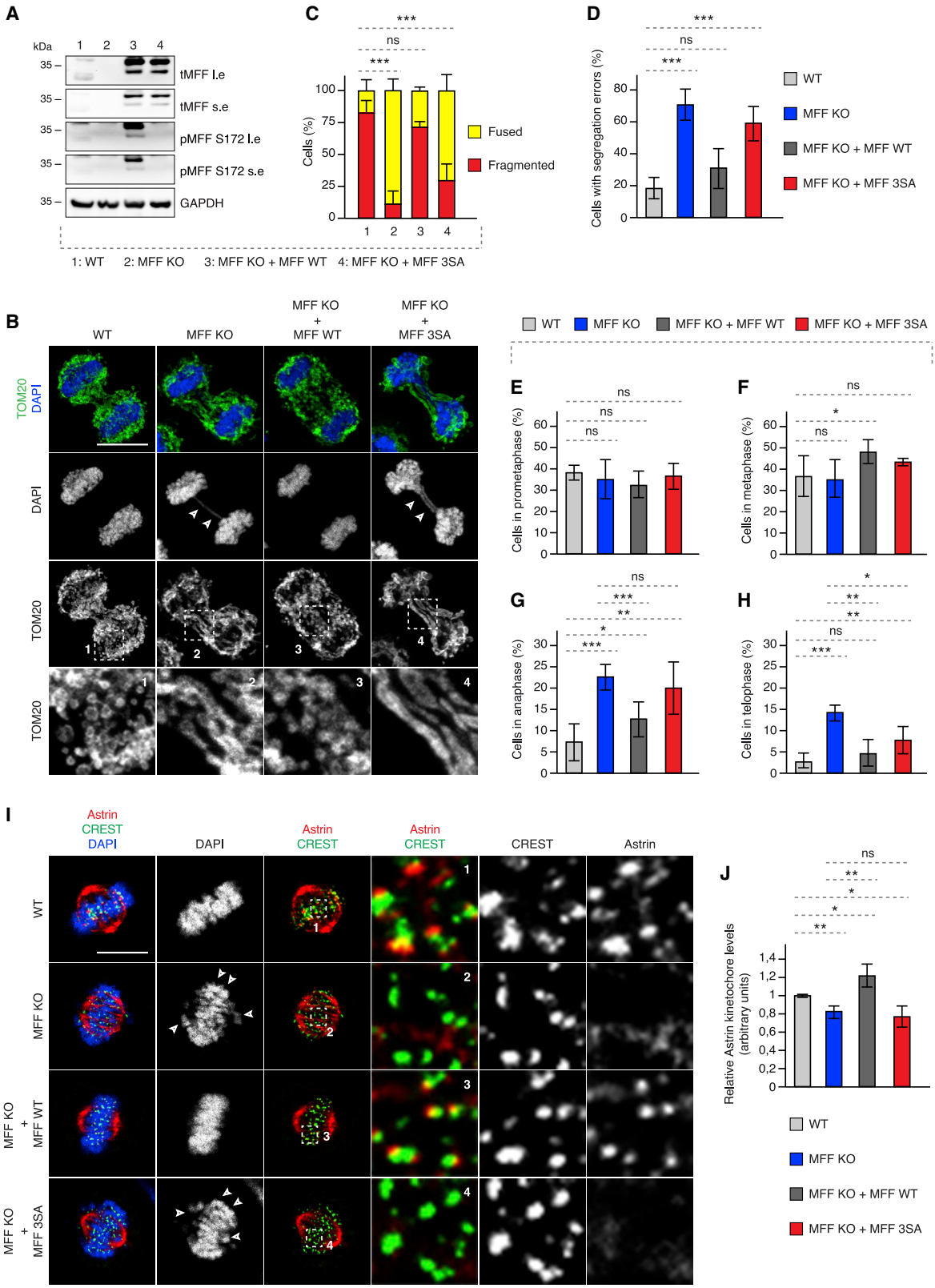

(legend on next page)

time for correction of chromosome alignment defects (Musacchio, 2015). Cells can escape the mitotic arrest, even when SAC is not satisfied, through a process called mitotic slippage or SAC adaptation.

It is well established that the loss of function of key SAC proteins, such as BubR1, diminishes SAC fidelity and consequently promotes polyploidy and genomic instability (Meraldi et al., 2004). The direct comparison of the mitotic defects in MFF KO cells and cells treated with specific siRNAs against BubR1 (Figure 6A) revealed a milder increase in polylobed nuclei in the absence of MFF (Figures 6B and 6C), whereas the chromosome segregation errors increased stronger in the absence of MFF than in BubR1-deficient cells (Figures 6B and 6D). These data suggest that MFF may promote SAC response, although not to the extent of a major SAC factor. This finding is in accordance with our live video analysis, in which MFF KO cells entered anaphase with a similar timing but before all chromosomes achieved bi-orientation at the mitotic spindle (Figures 1E and 1F) and with our analysis of the localization of the midzone marker PRC1 (Figure 1G).

To further test the hypothesis that PKD-dependent MFF phosphorylation may protect cells from SAC adaptation, we investigated cell fate and length of the mitotic arrest in the presence of the microtubule poison and SAC potentiating drug taxol. As expected, taxol treatment induced prolonged mitotic arrest and frequently led to apoptotic death in HeLa WT cells and in MFF KO cells expressing MFF WT (Figures 6E and 6F; Videos S1 and S2). In contrast, a significant number of MFF KO cells and MFF KO cells expressing MFF 3SA failed to sustain prolonged mitotic arrest and slipped out into polylobed nuclei-containing cells (Figures 6E, 6F, and 6G; Videos S3 and S4). The time spent in taxol-induced prometaphase-like stage was also reduced in MFF KO cells and MFF KO cells expressing MFF 3SA relative to WT cells and to MFF KO cells expressing MFF WT (Figure 6H). These data suggest that PKD-dependent MFF phosphorylation may protect cells from mitotic slippage in the presence of misaligned chromosomes.

PKD-dependent MFF phosphorylation fine-tunes levels of Cyclin B1

It has been proposed that mammalian cells can escape mitosis even in the presence of a functional mitotic checkpoint if Cyclin B1 levels fall below the threshold required to maintain the mitotic state (Brito and Rieder, 2006). Even a small drop in Cyclin B1 levels seems to be sufficient for reaching the critical threshold required for mitotic exit despite severe segregation errors (Gascoigne and Taylor, 2008). Considering that cells depleted for MFF and/or cells lacking PKD-mediated MFF phosphorylation display a predisposition for SAC adaptation (Figures 6E–6H), we first analyzed the localization of Cyclin B1 in metaphase-arrested cells. MFF KO cells and MFF KO cells expressing MFF 3SA displayed reduced levels of the cytoplasmic pool of Cyclin B1 (Figures 7A and 7B), but not the spindle associated pool (Figures 7A and 7C), relative to WT cells and to MFF KO cells expressing MFF WT. In line with this observation, reduced levels of Cyclin B1 could be observed in taxol-arrested cells acutely depleted for MFF by using siRNA relative to control conditions (Figure S7A). However, the accumulation of Cyclin B1 prior to the metaphase stage was independent of the presence of MFF and of its phosphorylation status (Figure S7B). Thus, MFF signaling may affect the stability of a very small pool of Cyclin B protein specifically during metaphase stage.

To further test this possibility, we analyzed the ubiquitylation of Cyclin B1 in metaphase-arrested cells in the presence of the proteasome inhibitor MG132. Immunoprecipitation of GFP-tagged Cyclin B1 under denaturing conditions revealed markedly increased polyubiquitin modification of Cyclin B1 in MFF KO cells relative to parental WT cells and to GFP-tag control immunoprecipitates (Figure 7D). Our results suggest that MFF-dependent signaling may affect ubiquitylation and possibly protein stability of a small cytoplasmic pool of Cyclin B1, thereby fine-tuning the SAC response in the presence of chromosome bi-orientation errors.

Existing evidence suggests that cells harboring accumulated segregation errors upon mitotic slippage often display reduced survival (Cheng and Crasta, 2017), and the long-term proliferation of aneuploid cancer cells is compromised upon inhibition of SAC (Cohen-Sharir et al., 2021; Quinton et al., 2021). Indeed, colony formation assays showed that the long-term proliferation capacity of MFF KO cells and of MFF KO cells expressing the non-phosphorylatable MFF 3SA was reduced relative to WT cells and MFF KO cells expressing WT MFF (Figures 7E and 7F). Thus, PKD-dependent phosphorylation of MFF may protect cells from SAC adaptation and promote cell survival.

Figure 5. PKD-dependent MFF phosphorylation drives mitotic mitochondrial fission and chromosome segregation

(A) WB of WT (1) and MFF KO (2) HeLa cells as well as MFF KO cells stably expressing WT MFF (3) or 3SA MFF (4) synchronized in mitosis under 16-h monastrol treatment.

(B–D) IF of WT and MFF KO HeLa cells as well as MFF KO cells stably expressing WT MFF or 3SA MFF synchronized for 16 h with monastrol in mitosis and collected 90 min after release from monastrol. ROIs are shown in the corresponding numbered panels. TOM20 was used as a mitochondrial marker, and chromosomes were stained with DAPI. Arrowheads point to DNA bridges. Scale bar, 5 μm. The percentage of cells with fragmented or fused mitochondrial morphology was quantified in (C), and the percentage of cells displaying segregation errors was quantified in (D). At least 300 cells per condition were analyzed (mean ± SD, ***$p < 0.001$, two-tailed t test, n = 3).

(E–H) WT and MFF KO HeLa cells as well as MFF KO cells stably expressing WT MFF or MFF 3SA MFF were treated as in (B), and the percentage of cells in different mitotic stages (prometaphase in E, metaphase in F, anaphase in G, and telophase in H) was quantified. At least 300 cells per condition were analyzed (mean ± SD, ***$p < 0.001$, **$p < 0.01$, *$p < 0.05$, two-tailed t test, n = 3).

(I and J) IF of WT and MFF KO HeLa cells as well as MFF KO cells stably expressing WT MFF or 3SA MFF synchronized for 16 h with monastrol in mitosis and collected 2 h after monastrol release into MG132. ROIs are shown in the corresponding numbered panels. Astrin (red) is associated with both kinetochores and microtubules. CREST was used as a kinetochore marker, and chromosomes were stained with DAPI. Arrowheads point to misaligned chromosomes. Scale bar, 5 μm. The relative intensity levels of Astrin on individual kinetochores were quantified in (J) as a readout for the stability of microtubule-kinetochore attachments by using the Fiji software. At least 200 cells per condition were analyzed (mean ± SD, **$p < 0.01$, *$p < 0.05$, two-tailed t test, n = 3).

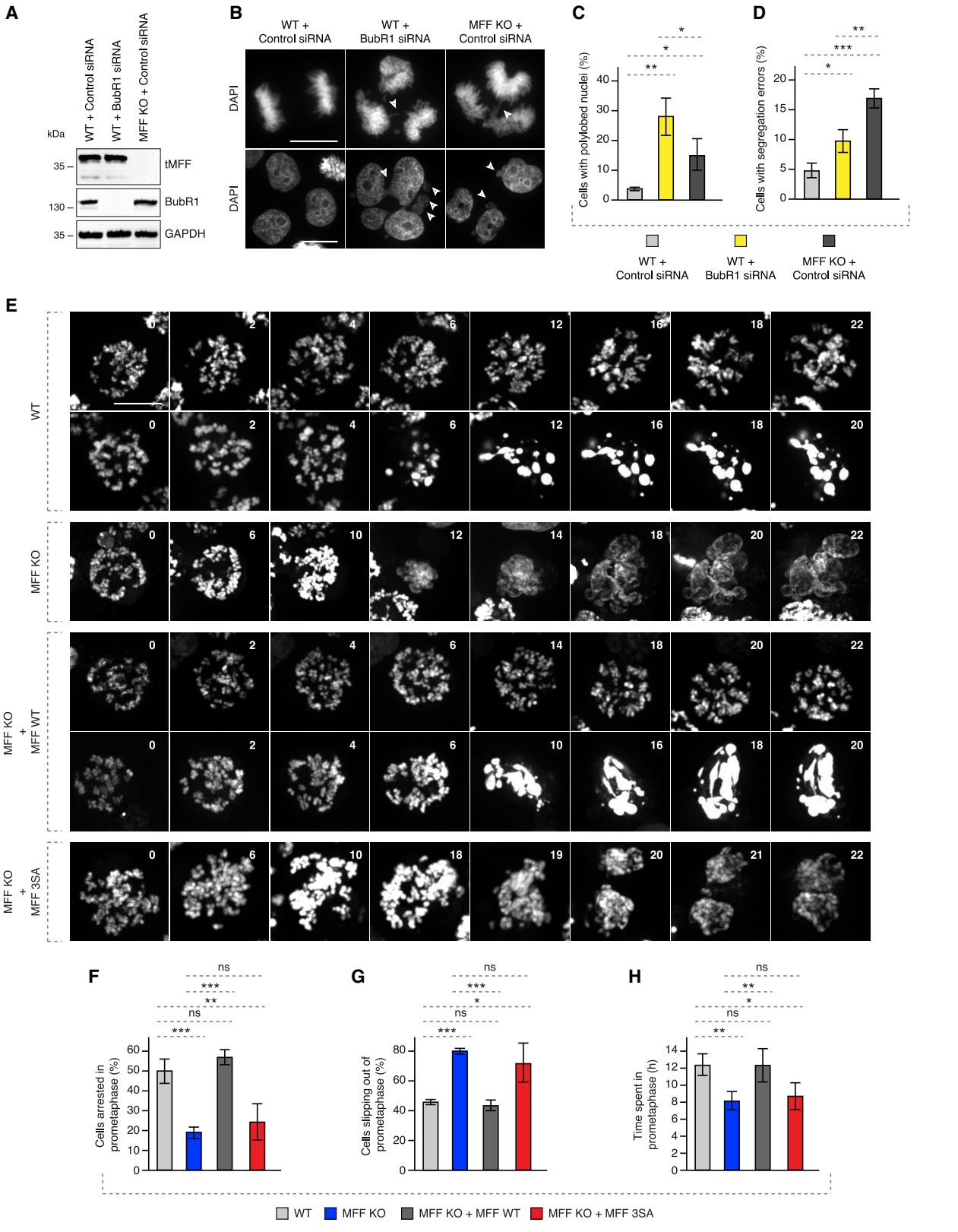

(legend on next page)

DISCUSSION

Taken together, our data suggest a model in which the PKD-MFF signaling couples mitochondrial fission to chromosome segregation during mitosis (Figure 7G). In normal cells, PKD directly phosphorylates MFF on serines 155, 172, and 275 and promotes mitochondrial fission specifically during mitosis. These phosphorylation events do not take place in interphase cells and are independent of the previously reported AMPK-dependent signaling occurring under low energy stress conditions (Toyama et al., 2016). MFF phosphorylation by PKD is crucial for accurate chromosome alignment and segregation and protects cells from adaptation to SAC in the presence of chromosome bi-orientation errors. We also demonstrate that PKD-MFF signaling is important for the maintenance of genome integrity and for cell survival. Upon deletion of PKD or MFF or in the absence of PKD-mediated MFF phosphorylation on serines 155, 172, and 275, mitochondrial fission is inhibited and cells initiate anaphase before chromosome bi-orientation on mitotic spindle is achieved, likely due to SAC adaptation. As a consequence, the absence of PKD-MFF signaling leads to chromosome segregation errors during anaphase, polylobed nuclei, and reduced long-term proliferation capacity (Figure 7G).

Emerging role of PKD in the regulation of mitotic energy homeostasis

Mitosis is a cellular process that demands high energy and requires tight spatiotemporal regulation to ensure genome integrity (Salazar-Roa and Malumbres, 2017). Functional mitochondria are required to meet the high energy demand that is needed to fuel the mitotic machinery (Kanfer and Kornmann, 2016). Given the role of AMPK in low energy sensing (Lin and Hardie, 2018) and in MFF-dependent mitochondrial fission in response to energy stress (Toyama et al., 2016), it is thus expected that AMPK activity is limited during late mitosis. This may explain why a different kinase is required for MFF phosphorylation and mitochondrial fission at this stage of cell division. It is interesting to note that AMPK is activated during early mitosis as a response to transient energy depletion to drive mitochondrial calcium flux, thereby restoring ATP production (Zhao et al., 2019). In contrast to AMPK, PKD is activated in the presence of energy-producing nutrients in different biological settings (Goginashvili et al., 2015; Sumara et al., 2009), indicating opposite functions in nutrient and energy sensing. It has also been demonstrated that PKD directly inactivates AMPK (Coughlan et al., 2016; Löffler et al., 2018), suggesting a potential crosstalk in response to energy changes during mitotic progression. Members of the PKD kinase family are well established regulators of fundamental cellular processes such as signal transduction, membrane trafficking, and secretion (Rozengurt, 2011). Interestingly, it has been reported that PKD can be dynamically localized to several mitotic structures (Papazyan et al., 2008) and that PKD inhibition delays cell cycle progression (Martínez-León et al., 2019; Roy et al., 2018). Our study provides further evidence that PKD represents an important mitotic kinase and extends the role of PKD to coupling of mitosis to the mitochondrial fission machinery. Several lines of evidence support the important role of PKD in mitochondrial fission and progression during mitosis. First, downregulation of PKD2 and PKD3 by specific siRNAs leads to mitochondrial fission defects and to chromosome alignment and segregation errors (Figures 2H–2J; Figures S4B and S4C). These phenotypes can be fully recapitulated in PKD2/3 dKO cells (Figure 3). Second, PKD can directly phosphorylate the MFF on serines 155, 172, and 275 during mitosis (Figure 4; Figure S5) independently of AMPK (Figure S5D). Finally, PKD-dependent phosphorylation of MFF is crucial for mitochondrial fission during mitosis but not in interphase and for accurate chromosome segregation during anaphase (Figures 5A–5H; Figures S6D and S6E). Interestingly, PKD1 has been demonstrated to be activated at mitochondria through formation of mitochondrial diacylglycerol (DAG) in response to oxidative stress (Cowell et al., 2009). In the future, it will be important to determine if mitotic activation of PKD (Figures 2D–2F) occurs specifically at mitochondria through localized synthesis of DAG.

Mitotic mitochondrial fission might be important for fidelity of chromosome segregation

Our data demonstrate that PKD phosphorylation is crucial for MFF-dependent mitochondrial fission specifically during mitosis, but it does not interfere with the ability of MFF to induce fragmentation in interphase (Figures 5B, 5D, S6D, and S6E). This finding suggests that phosphorylated MFF represents the main signaling trigger for mitotic mitochondrial fission and its function may not be compensated by other existing mitochondrial fission receptors. However, can the function of phosphorylated MFF in chromosome segregation be directly attributed to its role in mitochondrial fission? Or does its role in mitosis represent a "moonlighting" or unrelated function of MFF? Several arguments support the hypothesis that MFF-mediated mitochondrial fission plays a direct role during mitosis. First, the function of DRP1, the fission factor recruited to mitochondria by MFF, has already been linked to faithful cell division (Yamano and Youle, 2011), and MFF is the predominant DRP1 receptor in mammalian cells (Otera et al., 2010). In accordance, depletion of DRP1

Figure 6. PKD-dependent MFF phosphorylation protects cells from SAC adaptation

(A) WB of WT or MFF KO HeLa cells treated with the indicated siRNAs and synchronized in mitosis with double thymidine block and release.

(B–D) IF of WT and MFF KO HeLa cells treated as in (A). Arrowheads point to DNA bridges and/or polylobed nuclei. DNA was stained with DAPI. Scale bar, 5 μm. The percentage of cells with polylobed nuclei was quantified in (C), and the percentage of cells displaying segregation errors was quantified in (D). At least 200 cells per condition were analyzed (mean ± SD, ***$p < 0.001$, **$p < 0.01$, *$p < 0.05$, two-tailed t test, n = 3).

(E–H) Spinning disk time lapse microscopy of WT, MFF KO, and MFF KO HeLa cells stably expressing WT MFF or 3SA MFF synchronized in prometaphase with Taxol for 24 h and analyzed by spinning disk live-video microscopy for another 24 h. The selected frames of the movies are depicted, and time is shown in h. SiR-DNA was used to stain DNA. Scale bar, 5 μm. The percentage of cells in prolonged prometaphase arrest was quantified in (F). The percentage of cells slipping out of prometaphase arrest was quantified in (G). The average time (h) that cells spent in prometaphase arrest was quantified in (H). At least 70 cells per condition were analyzed (mean ± SD, ***$p < 0.001$, **$p < 0.01$, *$p < 0.05$, two-tailed t test, n = 3).

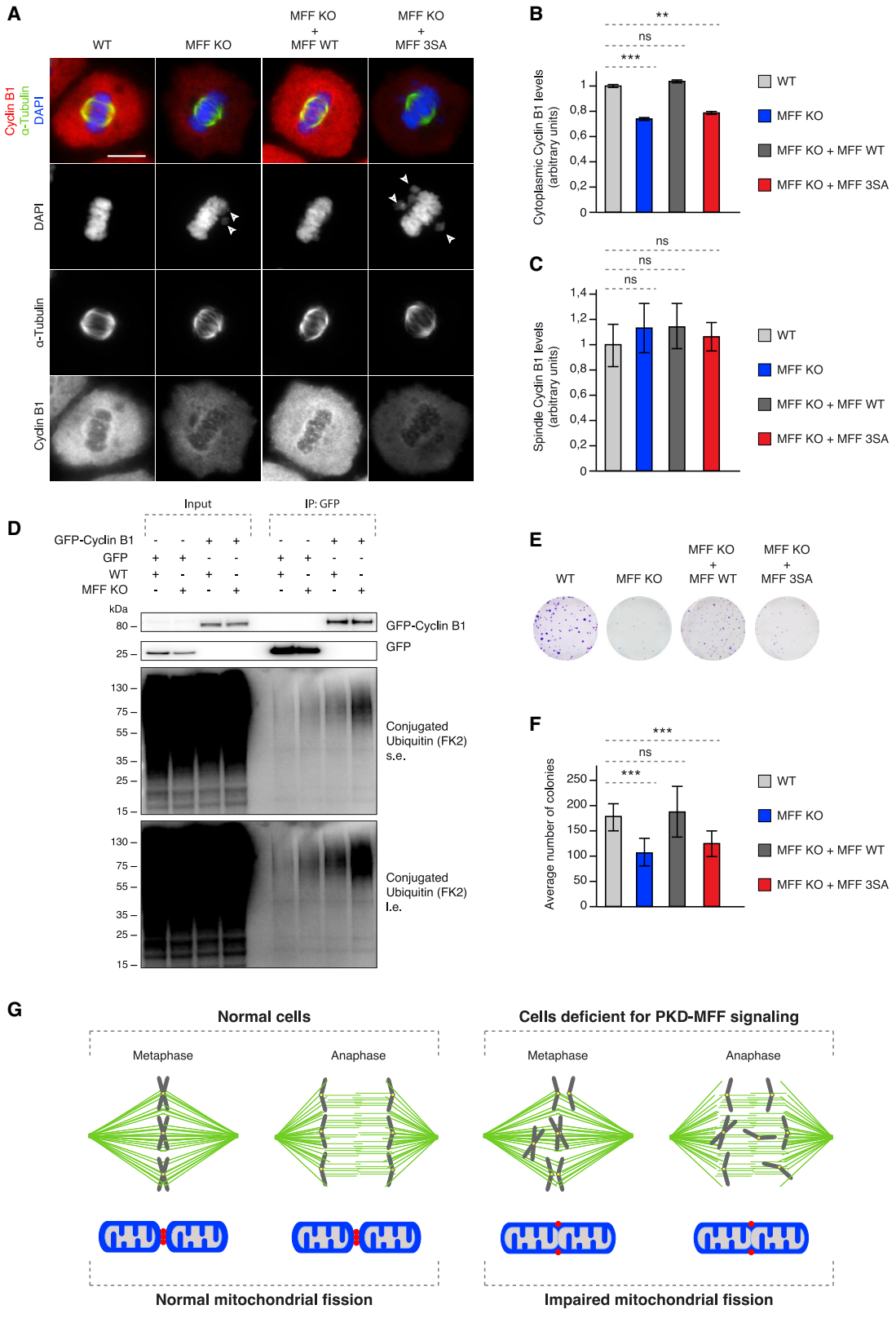

(legend on next page)

receptor MID49 did not result in segregation errors (Figures S3A–S3C), suggesting that MFF may act as a major DRP1 mitochondrial receptor in mitosis and may not be compensated by other receptors. Importantly, and also in our hands, DRP1 depletion yielded mitotic phenotypes including chromosome segregation errors (Figures S3A–S3C) and a polylobed nuclei phenotype (Figures S1B–S1E) of similar severity as the ones in MFF-depleted cells. Second, chromosomal segregation errors caused by MFF deficiency are fully rescued by concomitant impairment of the fusion machinery (Figures S3D–S3F), suggesting that counterbalancing defects in mitochondrial fission have direct a consequence on mitotic progression and that mitochondrial fission can be functionally coupled to mitotic fidelity. One caveat of the present study is that due to pandemic-associated restrictions, we were unable to determine whether disabling the fusion machinery could rescue the segregation errors in PKD-deficient cells, a result that would further strengthen our proposed model. In the future, it would also be worth investigating if, during mitosis, mitochondrial fusion factors could compete with MFF for phosphorylation by PKD.

Finally, although the mitochondrial membrane potential was not affected by MFF depletion (Figure S6F), ATP production was strongly reduced in MFF KO cells during mitosis but not in interphase (Figure S6G). Thus, chromosome segregation defects in MFF-deficient cells might be a consequence of lowered energy levels due to a lack of mitochondrial fission during mitosis and suggest a specific function of MFF-mediated mitochondrial fission in mitotic progression.

PKD-MFF signaling may protect mitotic cells from SAC adaptation

How exactly does PKD phosphorylated MFF regulate mitosis? Our data demonstrate that cells lacking PKD-, MFF-, or PKD-dependent phosphorylation of MFF fail to achieve bi-orientation of chromosomes at the mitotic spindle and proceed to anaphase onset in the presence of unaligned chromosomes (Figures 1E, 1G, and 3D). MFF phosphorylation appears to be also important for fine-tuning the stability of MT-KT attachments during mitosis (Figures 5I and 5J). Typically, in the absence of stable MT-KT attachments, the surveillance mechanism named SAC initiates an inhibitory signaling cascade to prevent anaphase onset, leading to prolonged mitotic arrest (Foley and Kapoor, 2013). Intriguingly, MFF-deficient cells do not delay the onset of anaphase and acquire chromosome segregation errors (Figures 1E–1H) and accumulate in the anaphase and telophase stages (Figures 1I, and 5E–5H). It is known that cells can escape the mitotic arrest, even in the presence of chromosome bi-orientation defects through a process called mitotic slippage or SAC adaptation. Indeed, PKD-dependent phosphorylation of MFF is important to sustain the SAC-mediated mitotic arrest induced by spindle poison taxol and may protect cells from the mitotic slippage (Figures 6E–6H; Videos S1, S2, S3, and S4). Even though the weak SAC response in MFF-deficient cells appears less pronounced than downregulation of one the main SAC effectors, BubR1 (Figures 6A–6D), we speculate that the PKD-MFF pathway promotes SAC response in mitotic cells. Interestingly, mice with BubR1 haploinsufficiency are rather prone to mitotic slippage and enhanced tumor development, whereas complete BubR1 KO mice are embryonically lethal (Dai et al., 2004; Wang et al., 2004), suggesting an ultrasensitive nature of the SAC response. It would be interesting to know if MFF-mediated SAC regulation can be mechanistically linked to the cellular energy homeostasis through mitochondrial fission. In this study, we speculate that PKD-dependent phosphorylation of MFF might be directly or indirectly involved in the regulation of a small pool of Cyclin B1. It is known that the anaphase promoting complex/cyclosome (APC/C)-dependent degradation of Cyclin B1 begins from its spindle-localized fractions (Clute and Pines, 1999), whereas in our hands, we observe a moderate reduction in a cytoplasmic fraction of Cyclin B1 in the absence of MFF phosphorylation, specifically in metaphase-arrested cells (Figures 7A–7C). This could explain the difficulty in detecting big differences in the total protein levels of Cyclin B1 by using biochemical analysis (Figure S7A). Another limitation of the present study, due to pandemic-associated restrictions, is that the levels of Cyclin B1 were not investigated in detail in DRP1-depleted cells, which also display severe segregation errors similar to MFF-depleted cells (Figures S3B and S3C). Because we were not able to detect changes in the total levels of Cyclin B1 in cells downregulated for DRP1 (Figure S7A), it would be important to monitor the relative Cyclin B1 levels by immunofluorescence (IF), as demonstrated for MFF-deficient cells (Figures 7A and 7B). Such experiments could further strengthen our proposed model and the causal link between mitochondrial fission and inhibition of mitotic slippage.

Nevertheless, even the small drop in Cyclin B1 levels detected in our hands by IF approaches could be capable of reaching the critical threshold required for mitotic slippage as it has been demonstrated previously (Gascoigne and Taylor, 2008). In addition,

Figure 7. PKD-dependent MFF phosphorylation fine-tunes levels of Cyclin B1

(A–C) IF of WT and MFF KO HeLa cells as well as MFF KO cells stably expressing WT MFF or 3SA MFF synchronized for 16 h with monastrol in mitosis and collected 2 h after monastrol release into MG132. α-Tubulin was used as a mitotic spindle marker, and chromosomes were stained with DAPI. Arrowheads point to misaligned chromosomes. Scale bar, 5 μm. The cytoplasmic Cyclin B1 levels and the relative intensity levels of Cyclin B1 on the mitotic spindle were quantified in (B) and in (C), respectively, by using the Fiji software. At least 300 cells per condition were analyzed (mean ± SD, $^{**}p < 0.01$, two-tailed t test, n = 3).

(D) WB of immunoprecipitations under denaturing conditions of WT and MFF KO HeLa cells transfected with plasmids encoding for GFP-CyclinB1 and His-Ubiquitin and synchronized as in (A). The s.e. and l.e. of the membrane blotted against the FK2 antibody that specifically recognizes conjugated but not free ubiquitin are shown.

(E and F) Colony-formation assay in WT MFF KO HeLa cells as well as MFF KO HeLa cells stably expressing WT MFF or 3SA MFF. Cells were kept in culture for 10 days, and the average number of colonies formed in each condition was quantified in (F) by using the Fiji software (mean ± SD, $^{***}p < 0.001$, two-tailed t test, n = 3).

(G) A hypothetical model describing how PKD-MFF phosphorylation affects mitotic progression and mitochondrial fission. In normal cells, PKD-MFF signaling ensures mitotic mitochondrial fission and fidelity of chromosome segregation. In cells deficient for PKD-MFF signaling, mitochondrial fission is impaired and chromosome segregation defects occur, likely due to adaptation to the mitotic checkpoint.

evidence exists for Cyclin B1 ubiquitin-mediated degradation by the E3-ubiquitin ligase $CRL2^{ZYG-11}$ that takes place independently of APC/C and facilitates mitotic slippage in a pathway conserved in *Caenorhabditis elegans* and in human cells (Balachandran et al., 2016). Given the strong increase in Cyclin B1 ubiquitylation in MFF-deficient cells, it is tempting to speculate that Cyclin B1 could display a higher affinity to $CRL2^{ZYG-11}$ than APC/C in the absence of the PKD-MFF signaling. Although future studies will have to identify the precise molecular mechanisms underlying the PKD-MFF-mediated SAC response, this pathway appears important for long-term proliferative capacity of cells (Figures 7E and 7F). Given that MFF was recently proposed to be required for tumor growth as a direct transcriptional target of the oncogenic Myc (Seo et al., 2019) and many aggressive cancers frequently show high levels of PKD activity (Guha et al., 2010), our findings on reduced survival in cells with a defective PKD-MFF pathway may also open unanticipated avenues in cancer research.

STAR★METHODS

Detailed methods are provided in the online version of this paper and include the following:

- KEY RESOURCES TABLE
- RESOURCE AVAILABILITY
  - Lead contact
  - Materials availability
  - Data and code availability
- EXPERIMENTAL MODEL AND SUBJECT DETAILS
  - Mice and MEFs
  - Generation of cell lines
  - Cell culture
- METHOD DETAILS
  - Cell cycle synchronization treatments
  - Cell treatments
  - Cloning and mutagenesis
  - Plasmid and siRNA transfections
  - Cell transfection and virus production
  - FACS analysis
  - WB
  - Fractionation
  - Immunoprecipitations
  - *In silico* PKD substrate identification
  - Recombinant protein expression and purification
  - *In vitro* kinase assay
  - Mass-spectrometry analysis
  - Cytospin and IF
  - Microscopy
  - Cell Counting and Categorization
  - ATP measurement
  - Mitochondrial Potential measurement
  - Colony Formation Assay
- QUANTIFICATION AND STATISTICAL ANALYSIS

SUPPLEMENTAL INFORMATION

Supplemental information can be found online at https://doi.org/10.1016/j.celrep.2021.109129.

ACKNOWLEDGMENTS

We thank G. Sumara and the members of the R.R. and I.S. laboratories for helpful discussions on the manuscript. We thank the IGBMC core facilities for their support on this research. We thank P. Koebel for purification of AAV viruses. E.P. was supported by a postdoctoral fellowship from the "Foundation pour la recherché Médicale" (FRM). O.B. was supported by Labex international PhD fellowship from IGBMC. Research in the I.S. laboratory was supported by IGBMC, CNRS, Fondation ARC pour la Recherche sur le Cancer (ARC), Institut National Du Cancer (INCa), Ligue Nationale contre le Cancer, USIAS, and Sanofi iAward Europe. Research in the R.R. laboratory was supported by FRM, Agence Nationale de la Recherche (ANR), and the European Foundation for the Study of Diabetes (EFSD)/Novo Nordisk Diabetes Research.

AUTHOR CONTRIBUTIONS

Conceptualization, supervision, and funding acquisition, I.S. and R.R.; methodology, validation, and formal analysis, E.P. and O.B.; investigation, E.P., O.B., L.G., S.S., A.A.-A., T.Y., Y.L., M.P.-G., E.C., Z.Z., and R.A.; software, E.G.; resources, C.K.; visualization, E.P., O.B., and I.S.; writing-review and editing, E.P., O.B., R.R., and I.S.

DECLARATION OF INTERESTS

The authors declare no competing interests.

Received: July 23, 2020
Revised: February 26, 2021
Accepted: April 22, 2021
Published: May 18, 2021

REFERENCES

Balachandran, R.S., Heighington, C.S., Starostina, N.G., Anderson, J.W., Owen, D.L., Vasudevan, S., and Kipreos, E.T. (2016). The ubiquitin ligase CRL2ZYG11 targets cyclin B1 for degradation in a conserved pathway that facilitates mitotic slippage. J. Cell Biol. *215*, 151–166.

Brito, D.A., and Rieder, C.L. (2006). Mitotic checkpoint slippage in humans occurs via cyclin B destruction in the presence of an active checkpoint. Curr. Biol. *16*, 1194–1200.

Britton, D., Zen, Y., Quaglia, A., Selzer, S., Mitra, V., Löβner, C., Jung, S., Böhm, G., Schmid, P., Prefot, P., et al. (2014). Quantification of pancreatic cancer proteome and phosphorylome: indicates molecular events likely contributing to cancer and activity of drug targets. PLoS One *9*, e90948.

Campeau, E., Ruhl, V.E., Rodier, F., Smith, C.L., Rahmberg, B.L., Fuss, J.O., Campisi, J., Yaswen, P., Cooper, P.K., and Kaufman, P.D. (2009). A versatile viral system for expression and depletion of proteins in mammalian cells. PLoS One *4*, e6529.

Chen, H., Ren, S., Clish, C., Jain, M., Mootha, V., McCaffery, J.M., and Chan, D.C. (2015). Titration of mitochondrial fusion rescues Mff-deficient cardiomyopathy. J. Cell Biol. *211*, 795–805.

Cheng, B., and Crasta, K. (2017). Consequences of mitotic slippage for antimicrotubule drug therapy. Endocr. Relat. Cancer *24*, T97–T106.

Cipolat, S., Martins de Brito, O., Dal Zilio, B., and Scorrano, L. (2004). OPA1 requires mitofusin 1 to promote mitochondrial fusion. Proc. Natl. Acad. Sci. USA *101*, 15927–15932.

Clute, P., and Pines, J. (1999). Temporal and spatial control of cyclin B1 destruction in metaphase. Nat. Cell Biol. *1*, 82–87.

Cohen-Sharir, Y., McFarland, J.M., Abdusamad, M., Marquis, C., Bernhard, S.V., Kazachkova, M., Tang, H., Ippolito, M.R., Laue, K., Zerbib, J., et al. (2021). Aneuploidy renders cancer cells vulnerable to mitotic checkpoint inhibition. Nature *590*, 486–491.

Coughlan, K.A., Valentine, R.J., Sudit, B.S., Allen, K., Dagon, Y., Kahn, B.B., Ruderman, N.B., and Saha, A.K. (2016). PKD1 Inhibits AMPKα2 through

Phosphorylation of Serine 491 and Impairs Insulin Signaling in Skeletal Muscle Cells. J. Biol. Chem. *291*, 5664–5675.

Cowell, C.F., Döppler, H., Yan, I.K., Hausser, A., Umezawa, Y., and Storz, P. (2009). Mitochondrial diacylglycerol initiates protein-kinase D1-mediated ROS signaling. J. Cell Sci. *122*, 919–928.

Dai, W., Wang, Q., Liu, T., Swamy, M., Fang, Y., Xie, S., Mahmood, R., Yang, Y.-M., Xu, M., and Rao, C.V. (2004). Slippage of mitotic arrest and enhanced tumor development in mice with BubR1 haploinsufficiency. Cancer Res. *64*, 440–445.

Díaz-Martínez, L.A., Karamysheva, Z.N., Warrington, R., Li, B., Wei, S., Xie, X.-J., Roth, M.G., and Yu, H. (2014). Genome-wide siRNA screen reveals coupling between mitotic apoptosis and adaptation. EMBO J. *33*, 1960–1976.

Döppler, H., Storz, P., Li, J., Comb, M.J., and Toker, A. (2005). A phosphorylation state-specific antibody recognizes Hsp27, a novel substrate of protein kinase D. J. Biol. Chem. *280*, 15013–15019.

Dunsch, A.K., Linnane, E., Barr, F.A., and Gruneberg, U. (2011). The astrin-kinastrin/SKAP complex localizes to microtubule plus ends and facilitates chromosome alignment. J. Cell Biol. *192*, 959–968.

Eiseler, T., Hausser, A., De Kimpe, L., Van Lint, J., and Pfizenmaier, K. (2010). Protein kinase D controls actin polymerization and cell motility through phosphorylation of cortactin. J. Biol. Chem. *285*, 18672–18683.

Fielitz, J., Kim, M.-S., Shelton, J.M., Qi, X., Hill, J.A., Richardson, J.A., Bassel-Duby, R., and Olson, E.N. (2008). Requirement of protein kinase D1 for pathological cardiac remodeling. Proc. Natl. Acad. Sci. USA *105*, 3059–3063.

Foley, E.A., and Kapoor, T.M. (2013). Microtubule attachment and spindle assembly checkpoint signalling at the kinetochore. Nat. Rev. Mol. Cell Biol. *14*, 25–37.

Franz-Wachtel, M., Eisler, S.A., Krug, K., Wahl, S., Carpy, A., Nordheim, A., Pfizenmaier, K., Hausser, A., and Macek, B. (2012). Global detection of protein kinase D-dependent phosphorylation events in nocodazole-treated human cells. Mol. Cell. Proteomics *11*, 160–170.

Gandre-Babbe, S., and van der Bliek, A.M. (2008). The novel tail-anchored membrane protein Mff controls mitochondrial and peroxisomal fission in mammalian cells. Mol. Biol. Cell *19*, 2402–2412.

Gascoigne, K.E., and Taylor, S.S. (2008). Cancer cells display profound intra- and interline variation following prolonged exposure to antimitotic drugs. Cancer Cell *14*, 111–122.

Gehart, H., Goginashvili, A., Beck, R., Morvan, J., Erbs, E., Formentini, I., De Matteis, M.A., Schwab, Y., Wieland, F.T., and Ricci, R. (2012). The BAR domain protein Arfaptin-1 controls secretory granule biogenesis at the trans-Golgi network. Dev. Cell *23*, 756–768.

Goginashvili, A., Zhang, Z., Erbs, E., Spiegelhalter, C., Kessler, P., Mihlan, M., Pasquier, A., Krupina, K., Schieber, N., Cinque, L., et al. (2015). Insulin granules. Insulin secretory granules control autophagy in pancreatic β cells. Science *347*, 878–882.

Guha, S., Tanasanvimon, S., Sinnett-Smith, J., and Rozengurt, E. (2010). Role of protein kinase D signaling in pancreatic cancer. Biochem. Pharmacol. *80*, 1946–1954.

Hausser, A., Storz, P., Märtens, S., Link, G., Toker, A., and Pfizenmaier, K. (2005). Protein kinase D regulates vesicular transport by phosphorylating and activating phosphatidylinositol-4 kinase IIIbeta at the Golgi complex. Nat. Cell Biol. *7*, 880–886.

Herst, P.M., Rowe, M.R., Carson, G.M., and Berridge, M.V. (2017). Functional Mitochondria in Health and Disease. Front. Endocrinol. (Lausanne) *8*, 296.

Jat, P.S., Cepko, C.L., Mulligan, R.C., and Sharp, P.A. (1986). Recombinant retroviruses encoding simian virus 40 large T antigen and polyomavirus large and middle T antigens. Mol. Cell. Biol. *6*, 1204–1217.

Jhun, B.S., O-Uchi, J., Adaniya, S.M., Mancini, T.J., Cao, J.L., King, M.E., Landi, A.K., Ma, H., Shin, M., Yang, D., et al. (2018). Protein kinase D activation induces mitochondrial fragmentation and dysfunction in cardiomyocytes. J. Physiol. *596*, 827–855.

Kanfer, G., and Kornmann, B. (2016). Dynamics of the mitochondrial network during mitosis. Biochem. Soc. Trans. *44*, 510–516.

Kashatus, D.F., Lim, K.-H., Brady, D.C., Pershing, N.L.K., Cox, A.D., and Counter, C.M. (2011). RALA and RALBP1 regulate mitochondrial fission at mitosis. Nat. Cell Biol. *13*, 1108–1115.

Kettenbach, A.N., Schweppe, D.K., Faherty, B.K., Pechenick, D., Pletnev, A.A., and Gerber, S.A. (2011). Quantitative phosphoproteomics identifies substrates and functional modules of Aurora and Polo-like kinase activities in mitotic cells. Sci. Signal. *4*, rs5.

Lee, L., Seager, R., Nakamura, Y., Wilkinson, K.A., and Henley, J.M. (2019). Parkin-mediated ubiquitination contributes to the constitutive turnover of mitochondrial fission factor (Mff). PLoS One *14*, e0213116.

Lewis, T.L., Jr., Kwon, S.-K., Lee, A., Shaw, R., and Polleux, F. (2018). MFF-dependent mitochondrial fission regulates presynaptic release and axon branching by limiting axonal mitochondria size. Nat. Commun. *9*, 5008.

Lin, S.-C., and Hardie, D.G. (2018). AMPK: Sensing Glucose as well as Cellular Energy Status. Cell Metab. *27*, 299–313.

Löffler, M.C., Mayer, A.E., Trujillo Viera, J., Loza Valdes, A., El-Merahbi, R., Ade, C.P., Karwen, T., Schmitz, W., Slotta, A., Erk, M., et al. (2018). Protein kinase D1 deletion in adipocytes enhances energy dissipation and protects against adiposity. EMBO J. *37*, e99182.

Losón, O.C., Song, Z., Chen, H., and Chan, D.C. (2013). Fis1, Mff, MiD49, and MiD51 mediate Drp1 recruitment in mitochondrial fission. Mol. Biol. Cell *24*, 659–667.

Malhotra, V., and Campelo, F. (2011). PKD regulates membrane fission to generate TGN to cell surface transport carriers. Cold Spring Harb. Perspect. Biol. *3*, a005280.

Martínez-León, E., Amable, G., Jácamo, R., Picco, M.E., Anaya, L., Rozengurt, E., and Rey, O. (2019). Protein kinase D1 inhibition interferes with mitosis progression. J. Cell. Physiol. *234*, 20510–20519.

Meraldi, P., Draviam, V.M., and Sorger, P.K. (2004). Timing and checkpoints in the regulation of mitotic progression. Dev. Cell *7*, 45–60.

Mertins, P., Mani, D.R., Ruggles, K.V., Gillette, M.A., Clauser, K.R., Wang, P., Wang, X., Qiao, J.W., Cao, S., Petralia, F., et al.; NCI CPTAC (2016). Proteogenomics connects somatic mutations to signalling in breast cancer. Nature *534*, 55–62.

Mollinari, C., Kleman, J.-P., Jiang, W., Schoehn, G., Hunter, T., and Margolis, R.L. (2002). PRC1 is a microtubule binding and bundling protein essential to maintain the mitotic spindle midzone. J. Cell Biol. *157*, 1175–1186.

Musacchio, A. (2015). The Molecular Biology of Spindle Assembly Checkpoint Signaling Dynamics. Curr. Biol. *25*, R1002–R1018.

Olsen, J.V., Vermeulen, M., Santamaria, A., Kumar, C., Miller, M.L., Jensen, L.J., Gnad, F., Cox, J., Jensen, T.S., Nigg, E.A., et al. (2010). Quantitative phosphoproteomics reveals widespread full phosphorylation site occupancy during mitosis. Sci. Signal. *3*, ra3.

Otera, H., Wang, C., Cleland, M.M., Setoguchi, K., Yokota, S., Youle, R.J., and Mihara, K. (2010). Mff is an essential factor for mitochondrial recruitment of Drp1 during mitochondrial fission in mammalian cells. J. Cell Biol. *191*, 1141–1158.

Otera, H., Ishihara, N., and Mihara, K. (2013). New insights into the function and regulation of mitochondrial fission. Biochim. Biophys. Acta *1833*, 1256–1268.

Papazyan, R., Doche, M., Waldron, R.T., Rozengurt, E., Moyer, M.P., and Rey, O. (2008). Protein kinase D isozymes activation and localization during mitosis. Exp. Cell Res. *314*, 3057–3068.

Park, Y.-Y., and Cho, H. (2012). Mitofusin 1 is degraded at G2/M phase through ubiquitylation by MARCH5. Cell Div. *7*, 25.

Peña-Blanco, A., Haschka, M.D., Jenner, A., Zuleger, T., Proikas-Cezanne, T., Villunger, A., and García-Sáez, A.J. (2020). Drp1 modulates mitochondrial stress responses to mitotic arrest. Cell Death Differ. *27*, 2620–2634.

Quinton, R.J., DiDomizio, A., Vittoria, M.A., Kotýnková, K., Ticas, C.J., Patel, S., Koga, Y., Vakhshoorzadeh, J., Hermance, N., Kuroda, T.S., et al. (2021). Whole-genome doubling confers unique genetic vulnerabilities on tumour cells. Nature *590*, 492–497.

Roy, A., Veroli, M.V., Prasad, S., and Wang, Q.J. (2018). Protein Kinase D2 Modulates Cell Cycle By Stabilizing Aurora A Kinase at Centrosomes. Mol. Cancer Res. *16*, 1785–1797.

Rozengurt, E. (2011). Protein kinase D signaling: multiple biological functions in health and disease. Physiology (Bethesda) *26*, 23–33.

Salazar-Roa, M., and Malumbres, M. (2017). Fueling the Cell Division Cycle. Trends Cell Biol. *27*, 69–81.

Schmitz, M.H.A., and Gerlich, D.W. (2009). Automated live microscopy to study mitotic gene function in fluorescent reporter cell lines. Methods Mol. Biol. *545*, 113–134.

Seo, J.H., Agarwal, E., Chae, Y.C., Lee, Y.G., Garlick, D.S., Storaci, A.M., Ferrero, S., Gaudioso, G., Gianelli, U., Vaira, V., and Altieri, D.C. (2019). Mitochondrial fission factor is a novel Myc-dependent regulator of mitochondrial permeability in cancer. EBioMedicine *48*, 353–363.

Silva Ramos, E., Motori, E., Brüser, C., Kühl, I., Yeroslaviz, A., Ruzzenente, B., Kauppila, J.H.K., Busch, J.D., Hultenby, K., Habermann, B.H., et al. (2019). Mitochondrial fusion is required for regulation of mitochondrial DNA replication. PLoS Genet. *15*, e1008085.

Sumara, G., Formentini, I., Collins, S., Sumara, I., Windak, R., Bodenmiller, B., Ramracheya, R., Caille, D., Jiang, H., Platt, K.A., et al. (2009). Regulation of PKD by the MAPK p38delta in insulin secretion and glucose homeostasis. Cell *136*, 235–248.

Taguchi, N., Ishihara, N., Jofuku, A., Oka, T., and Mihara, K. (2007). Mitotic phosphorylation of dynamin-related GTPase Drp1 participates in mitochondrial fission. J. Biol. Chem. *282*, 11521–11529.

Toyama, E.Q., Herzig, S., Courchet, J., Lewis, T.L., Jr., Losón, O.C., Hellberg, K., Young, N.P., Chen, H., Polleux, F., Chan, D.C., and Shaw, R.J. (2016). Metabolism. AMP-activated protein kinase mediates mitochondrial fission in response to energy stress. Science *351*, 275–281.

Vader, G., Maia, A.F., and Lens, S.M. (2008). The chromosomal passenger complex and the spindle assembly checkpoint: kinetochore-microtubule error correction and beyond. Cell Div. *3*, 10.

Wang, Q., Liu, T., Fang, Y., Xie, S., Huang, X., Mahmood, R., Ramaswamy, G., Sakamoto, K.M., Darzynkiewicz, Z., Xu, M., and Dai, W. (2004). BUBR1 deficiency results in abnormal megakaryopoiesis. Blood *103*, 1278–1285.

Wieckowski, M.R., Giorgi, C., Lebiedzinska, M., Duszynski, J., and Pinton, P. (2009). Isolation of mitochondria-associated membranes and mitochondria from animal tissues and cells. Nat. Protoc. *4*, 1582–1590.

Yamano, K., and Youle, R.J. (2011). Coupling mitochondrial and cell division. Nat. Cell Biol. *13*, 1026–1027.

Yeaman, C., Ayala, M.I., Wright, J.R., Bard, F., Bossard, C., Ang, A., Maeda, Y., Seufferlein, T., Mellman, I., Nelson, W.J., and Malhotra, V. (2004). Protein kinase D regulates basolateral membrane protein exit from trans-Golgi network. Nat. Cell Biol. *6*, 106–112.

Yi, T., Zhai, B., Yu, Y., Kiyotsugu, Y., Raschle, T., Etzkorn, M., Seo, H.-C., Nagiec, M., Luna, R.E., Reinherz, E.L., et al. (2014). Quantitative phosphoproteomic analysis reveals system-wide signaling pathways downstream of SDF-1/CXCR4 in breast cancer stem cells. Proc. Natl. Acad. Sci. USA *111*, E2182–E2190.

Yu, R., Liu, T., Jin, S.-B., Ning, C., Lendahl, U., Nistér, M., and Zhao, J. (2017). MIEF1/2 function as adaptors to recruit Drp1 to mitochondria and regulate the association of Drp1 with Mff. Sci. Rep. *7*, 880.

Yuan, J., Rey, O., and Rozengurt, E. (2006). Activation of protein kinase D3 by signaling through Rac and the alpha subunits of the heterotrimeric G proteins G12 and G13. Cell. Signal. *18*, 1051–1062.

Zhang, Z., Meszaros, G., He, W.T., Xu, Y., de Fatima Magliarelli, H., Mailly, L., Mihlan, M., Liu, Y., Puig Gámez, M., Goginashvili, A., et al. (2017). Protein kinase D at the Golgi controls NLRP3 inflammasome activation. J. Exp. Med. *214*, 2671–2693.

Zhao, H., Li, T., Wang, K., Zhao, F., Chen, J., Xu, G., Zhao, J., Li, T., Chen, L., Li, L., et al. (2019). AMPK-mediated activation of MCU stimulates mitochondrial Ca^{2+} entry to promote mitotic progression. Nat. Cell Biol. *21*, 476–486.

STAR★METHODS

KEY RESOURCES TABLE

REAGENT or RESOURCE	SOURCE	IDENTIFIER
Antibodies		
Rabbit polyclonal anti-MFF	This study	N/A
Rabbit polyclonal anti-phospho-Ser155 MFF	This study	N/A
Rabbit polyclonal anti- phospho-Ser275 MFF	This study	N/A
Mouse monoclonal anti-GFP	This study	N/A
Mouse monoclonal anti-GST	This study	N/A
Rabbit polyclonal anti-Phospho-MFF (Ser172)	Cell Signaling Technology	Cat# 49281, RRID:AB_2799354
Rabbit polyclonal anti-Phospho-PKD/PKCmu (Ser916)	Cell Signaling Technology	Cat# 2051, RRID:AB_330841
Rabbit polyclonal anti-Phospho-PKD/PKCmu (Ser744/748)	Cell Signaling Technology	Cat# 2054, RRID:AB_2172539
Rabbit polyclonal anti-Anti-PKD, phospho (Ser / Thr)	Cell Signaling Technology	Cat# 4381, RRID:AB_1264239
Rabbit polyclonal anti-PKD/PKCmu	Cell Signaling Technology	Cat# 2052, RRID:AB_2268946
Rabbit monoclonal anti-PKD2 (D1A7)	Cell Signaling Technology	Cat# 8188, RRID:AB_10829368
Rabbit monoclonal anti-PKD3/PKC (D57E6)	Cell Signaling Technology	Cat# 5655, RRID:AB_10695917
Rabbit monoclonal anti-AMPK-alpha, phospho (Thr172)	Cell Signaling Technology	Cat# 2535, RRID:AB_331250
Rabbit polyclonal anti-AMPK-alpha	Cell Signaling Technology	Cat# 2532, RRID:AB_330331
Rabbit monoclonal anti-Phospho-ULK1 (Ser555) (D1H4)	Cell Signaling Technology	Cat# 5869, RRID:AB_10707365
Rabbit polyclonal anti-ULK1 (A705)	Cell Signaling Technology	Cat# 4776, RRID:AB_2212518
Rabbit monoclonal anti-Phospho-Acetyl-CoA Carboxylase (Ser79) (D7D11)	Cell Signaling Technology	Cat# 11818, RRID:AB_2687505
Rabbit polyclonal anti-Acetyl-CoA Carboxylase 1	Cell Signaling Technology	Cat# 4190, RRID:AB_10547752
Rabbit monoclonal anti-DRP1 (D6C7)	Cell Signaling Technology	Cat# 8570, RRID:AB_10950498
Rabbit polyclonal anti-Phospho-Histone H3 (Ser10)	Cell Signaling Technology	Cat# 9701, RRID:AB_331535
Rabbit polyclonal anti-PKC mu (C-20)	Santa Cruz Biotechnology	Cat# sc-639, RRID:AB_2172392
Rabbit polyclonal anti-Tom20 (FL-145)	Santa Cruz Biotechnology	Cat# sc-11415, RRID:AB_2207533
Mouse monoclonal anti-Tom20 (F-10)	Santa Cruz Biotechnology	Cat# sc-17764, RRID:AB_628381
Mouse monoclonal anti-PRC1 (6G2)	Santa Cruz Biotechnology	Cat# sc-56345, RRID:AB_630139
Mouse monoclonal anti-Cyclin B1 (G-11)	Santa Cruz Biotechnology	Cat# sc-166757, RRID:AB_2072277
Mouse monoclonal ANTI-FLAG® M2	Sigma-Aldrich	Cat# F1804, RRID:AB_262044
Rabbit polyclonal Anti-GAPDH	Sigma-Aldrich	Cat# G9545, RRID:AB_796208
Mouse monoclonal Anti-α-Tubulin	Sigma-Aldrich	Cat# T9026, RRID:AB_477593
Rabbit polyclonal anti-BUBR1	Thermo Fisher Scientific	Cat# 720297, RRID:AB_2610165
Rabbit polyclonal anti-Cyclin B1	Proteintech	Cat# 55004-1-AP, RRID:AB_10859790
Rabbit polyclonal anti-UQCC2 (MFN1)	Proteintech	Cat# 25781-1-AP, RRID:AB_2880237
Rabbit polyclonal anti-SMCR7 (MID49)	Proteintech	Cat# 28718-1-AP, RRID:AB_2881198
Human polyclonal anti-Centromere	Antibodies Incorporated	Cat# 15-234-0001, RRID:AB_2687472
Mouse monoclonal anti-Ubiquitin (FK2)	Millipore	Cat# ST1200 100UG, RRID:AB_10681625
Rabbit polyclonal anti-Astrin	Ulrike Gruneberg (Cancer Research, UK)	N/A

(*Continued on next page*)

Continued

REAGENT or RESOURCE	SOURCE	IDENTIFIER
Bacterial and virus strains		
BL21 (DE3) Competent *E. coli*	NEW ENGLAND BioLabs	Cat#c2527h
DH5alpha Competent *E. coli*	NEW ENGLAND BioLabs	Cat# C2987I
Stbl3 Competent *E. coli*	Thermo Fisher Scientific	Cat #C737303
rAAV2/DJ	Cell Biolabs	Cat. No. VPK-430-DJ
Chemicals, peptides, and recombinant proteins		
Rotenone	Sigma-Aldrich	Cat# R8875
Carbonyl cyanide 3-chlorophenylhydrazone, CCCP	Sigma-Aldrich	Cat# C2759
Antimycin A	Sigma-Aldrich	Cat# A8674
Thymidine	Sigma-Aldrich	Cat# T1895-5G
Nocodazole	Sigma-Aldrich	Cat# M-1404
Paclitaxel	Sigma-Aldrich	Cat# T-7191
Monastrol	Sigma-Aldrich	Cat# M8515
RO-3306	Sigma-Aldrich	Cat# SML0569
4′,6-Diamidino-2-phenylindole dihydrochloride (DAPI)	Sigma-Aldrich	Cat# D8417
CRT 0066101	Tocris Bioscience	Cat#4975
MG132	Tocris Bioscience	Cat#1748
STLC (S-Trityl-L-cysteine)	Enzo Life Sciences	Cat# ALX-105-011-M500
Mitotracker-Green FM	Thermo Fischer Scientific	Cat# M7514
MOWIOL 4-88 Reagent	Millipore	Cat# 475904-M
jetPEI®	Polyplus transfection	Cat# 101-01N
SiR-DNA	Sprirochrom	Cat#SC007
Polybrene	Santa Cruz	Cat# sc-134220
Recombinant human GST-PKD1	Enzo Life Sciences	Cat# BML-SE348-0005
Critical commercial assays		
ATP Assay Kit	Abcam	Cat# ab83355
JC-1 - Mitochondrial Membrane Potential Assay Kit	Abcam	Cat# ab113850
Experimental models: Cell lines		
Human: HeLa-H2B-mCherry/MTS-EGFP	Schmitz and Gerlich, 2009	N/A
Human: HEK293T-AMPK α1/α2 dKO	This study	N/A
Human: HeLa-MFF KO	This study	N/A
Human: HEK293T-MFF KO	This study	N/A
Human: HeLa-PKD2/3 dKO	This study	N/A
Human: HeLa-FLAG (pLenti-CMV-Blast)	This study	N/A
Human: HeLa-MFF KO-FLAG (pLenti-CMV-Blast)	This study	N/A
Human: HeLa-MFF KO-FLAG-MFF WT (pLenti-CMV-Blast)	This study	N/A
Human: HeLa-MFF KO-FLAG-MFF 3SA (pLenti-CMV-Blast)	This study	N/A
Human: HEK293T embryonic kidney	ATCC	Cat#CRL-1573
Human: HeLa cervix adenocarcinoma	ATCC	Cat#CCL-2
Human: Phoenix Eco HEK293T Retrovirus packaging	Orbigen Inc., a gift from H. Groenemeyer, IGBMC	N/A
Human: U2OS bone osteosarcoma	ATCC	Cat#HTB-96
Mouse embryonic fibroblasts (MEFs) PKD1/3 fl/fl	This study	N/A

(*Continued on next page*)

Continued

REAGENT or RESOURCE	SOURCE	IDENTIFIER
Experimental models: Organisms		
PKD1 floxed (PKD1fl/fl) mice	Fielitz et al., 2008; Zhang et al., 2017	N/A
PKD3 floxed (PKD3fl/fl) mice	Fielitz et al., 2008; Zhang et al., 2017	N/A
Oligonucleotides		
siRNA: Non-targeting	Dharmacon	Cat#D-001210-02-05
siRNA: DNM1L (DRP1) smartpool	Dharmacon	Cat#L-012092-00-0005
siRNA: OPA1 smartpool	Dharmacon	Cat#L-005273-00-0005
siRNA: MFF smartpool	Dharmacon	Cat#L-018261-00-0005
siRNA: UQCC2 (MFN1) smartpool	Dharmacon	Cat#L-021290-02-0005
siRNA: MIEF2 (MID49) smartpool	Dharmacon	Cat#L-017272-02-0005
siRNA: BUB1B (BUBR1) smartpool	Dharmacon	Cat#L-004101-00-0005
siRNA: PRKD2 smartpool	Dharmacon	Cat#L-004197-00-0005
siRNA: PRKD3 smartpool	Dharmacon	Cat#L-005029-00-0005
shRNA: mouse PRKD2 CCGGGAAA CTGCTCAAGGGTCTATTCTCGAGAA TAGACCCTTGAGCAGTTTCTTTTTG	This study	N/A
Primers used for Cloning, Subcloning and Mutagenesis are described in Table S1	This study	N/A
Recombinant DNA		
pcDNA3.1/Zeo(+)	Thermo Fischer Scientific	Cat#V79020
pcDNA3.1-FLAG-MFF WT (291 a.a.)	This study	N/A
pcDNA3.1-FLAG-MFF WT (218 a.a.)	This study	N/A
pcDNA3.1-FLAG-MFF S155A	This study	N/A
pcDNA3.1-FLAG-MFF S172A	This study	N/A
pcDNA3.1-FLAG-MFF S275A	This study	N/A
pcDNA3.1-FLAG-MFF S155AS172A	This study	N/A
pcDNA3.1-FLAG-MFF S155AS275A	This study	N/A
pcDNA3.1-FLAG-MFF S172AS275A	This study	N/A
pcDNA3.1-FLAG-MFF S155AS172AS275A (3SA)	This study	N/A
pGEX6P1	GE Healthcare Life Sciences	Cat#27-1542-01
pGEX6P1-MFF (291 a.a. ΔTM) WT	This study	N/A
pGEX6P1-MFF ΔTM S155A	This study	N/A
pGEX6P1-MFF ΔTM S172A	This study	N/A
pGEX6P1-MFF ΔTM S275A	This study	N/A
pGEX6P1-MFF ΔTM S155AS172A	This study	N/A
pGEX6P1-MFF ΔTM S155AS275A	This study	N/A
pGEX6P1-MFF ΔTM S172AS275A	This study	N/A
pGEX6P1-MFF ΔTM S155AS172AS275A (3SA)	This study	N/A
pGEX6P1-MFF ΔTM S155AS172AT112A	This study	N/A
pGEX6P1-MFF ΔTM S155AT280AT112AY39F	This study	N/A
pGEX6P1-MFF ΔTM S155AS172AT112AS275A	This study	N/A
pEGFP-N1	Clontech	Cat#6085-1
pEGFP-PKD1 WT	Gehart et al., 2012	N/A
pEGFP-PKD1 CA	Gehart et al., 2012	N/A
pEGFP-PKD1 KD	Gehart et al., 2012	N/A
pEGFP-PKD2 WT	This study	N/A
pLenti CMV Blast empty	Campeau et al., 2009	Addgene Cat#17486

(*Continued on next page*)

Continued		
REAGENT or RESOURCE	SOURCE	IDENTIFIER
pLenti CMV Blast-MFF WT	This study	N/A
pLenti CMV Blast-MFF 3SA	This study	N/A
Software and algorithms		
CRISPR/Cas9 Guide RNA Design	GPP Web Portal, Broad Institute, Cambridge, MA, USA	https://portals.broadinstitute.org/gpp/public/analysis-tools/sgrna-design
Fiji Image Analysis	ImageJ	https://imagej.net/Fiji
Prism version 8.1.1	GraphPad	N/A

RESOURCE AVAILABILITY

Lead contact

Further information and request for resources should be directed to and will be fulfilled by the Lead Contact, Izabela Sumara (sumara@igbmc.fr).

Materials availability

Materials, including plasmids and cell lines, are available from the authors upon request.

Data and code availability

The published article includes data generated in this study, no unique software or code were generated for this study.

EXPERIMENTAL MODEL AND SUBJECT DETAILS

Mice and MEFs

PKD1 floxed (PKD1fl/fl) and PKD3 floxed (PKD3fl/fl) mice were described previously (Fielitz et al., 2008; Zhang et al., 2017). PKD1fl/fl mice were provided by E.N. Olson (University of Texas Southwestern). PKD3fl/fl mice were provided by M. Leitges (Biotechnology Centre of Oslo). As PKD1 knockout mice are embryonically lethal (Fielitz et al., 2008), we generated PKD1-PKD3 fl/fl mice by crossing PKD1fl/fl mice and PKD3fl/fl mice on C57BL/6J background. Mice were housed on a 12-h light/dark cycle and received standard chow diet in the animal facility of the IGBMC in compliance with the European legislation on care and use of laboratory animals. For PKD1/PKD3 dKO MEFs generation, Mouse Embryonic Fibroblasts (MEFs) were isolated from 12.5-day-old embryos of PKD1-PKD3 fl/fl mice. Early (1-4) passages were frozen. To generate the PKD1-PKD3 DKO MEFs, early passage PKD1-PKD3 fl/fl MEFs were infected with retroviral vector pZip-Neo-SV(X)1 containing SV40 large T antigen (Addgene: 1776) (Jat et al., 1986) (a kind gift from H. Groenemeyer, IGBMC). Infected cells were selected for viral integration using 0.5 mg/mL neomycin (G418) for 3 days until there were no cells remained on the control plate. Transformed PKD1-PKD3 fl/fl MEFs were propagated and later infected with Adeno-associated viruses encoding either eGFP (control) or Cre-eGFP (AAV-CMV-eGFP or AAV-CMV-Cre-eGFP) using rAAV2/DJ vectors from AAV Helper Free System (Cat. No. VPK-430-DJ) from Cell Biolabs. Briefly, 40 μL of the virus (AAV-CMV-eGFP or AAV-CMV-Cre-eGFP) were added in the new media in 1 well of a 6 well plate, containing cells at 20%–30% confluency. After 48h the cells were split in 10cm dish and allowed to grow until confluent. To ensure the purity, infected cells were selected for GFP or Cre-GFP expression using FACS. Efficient PKD1/3 deletions were validated by WB and by genotyping PCR. To generate PKD1/3 MEFs lacking PKD2 and corresponding scrambled controls PKD1/3 MEFs were further infected with pLKO.1-puro lentiviral vectors containing shRNA against mouse PKD2 or scrambled control. Infected cells were selected using puromycin at the concentration of 1 μg/ml until there were no cells remaining on the control plate (7 days). Downregulation of PKD2 was confirmed by WB.

Generation of cell lines

Stable monoclonal reporter cell line (HeLa-H2B-mCherry/MTS-EGFP) was generated as previously described (Schmitz and Gerlich, 2009).

AMPK α1/α2 DKO HEK293T cell line was generated using CRISPR/Cas9 genome editing system as described previously (Toyama et al., 2016) except for pX330-P2A-EGFP and pX330-P2A-RFP vectors were used instead of pX462 vector with puromycin selection. 24 hours after transfection GFP/RFP double positive cells were single-sorted into 96-well plates by FACS. Single clones were validated by light microscopy and screened for AMPK α1/α2 proteins by WB.

MFF KO HeLa and HEK293T cell lines were generated using CRISPR/Cas9 genome editing system. Two guide RNA sequences (5′-TAGTCGAATTCAGTACGAAA-3′, gRNA1 and 5′-TGATAATGCAAGTTCCGGAG-3′, gRNA2) were cloned into pX330-P2A-EGFP and pX330-P2A-RFP by annealing and ligation using T4 ligase. 24 hours after transfection GFP/RFP double positive cells were

single-sorted into 96-well plates by FACS. Single clones were validated by light microscopy and screened for MFF proteins by WB. Clones were genotyped and sequenced by Sanger sequencing (GATC).

PKD2/3 dKO HeLa cell line was generated using CRISPR/Cas9 genome editing system. Two guide RNA sequences for PKD2 (5′-TCGAGGACTTCCAGATCCGC-3′, gRNA1 and 5′-CACGGTGCACTCCTATCGGG-3′, gRNA2) and PKD3 (5′ATAAATAGTGATAGT AGTCG −3′, gRNA1 and 5′-GGATCCATCTGATCTCGATG-3′, gRNA2) were cloned into pX330-P2A-EGFP and pX330-P2A-RFP by annealing and ligation using T4 ligase. 24 hours after transfection GFP/RFP double positive cells were single-sorted into 96-well plates by FACS. Single clones were validated by light microscopy and screened for PKD2/3 proteins by WB. Clones were genotyped and sequenced by Sanger sequencing (GATC).

To generate the stable cell lines HeLa WT and MFF KO cell lines were infected with lentivirus based on pLenti-CMV-Blast vector carrying Flag-tagged human WT MFF, 3SA MFF mutant or empty viral vector. Transduced cells were selected for viral integration using blasticidin at the concentration of 5 μg/mL for 10 days. Resistant cells were analyzed for MFF expression using immunoblot and used as pools of cells for experiments.

Cell culture

All cell lines were maintained at 37°C in 5% CO_2 humidified incubator. HeLa Kyoto human cervix carcinoma cells (gift from S. Narumiya (Kyoto University, Kyoto, Japan) and all their derived KO or stable cell lines were grown in high glucose DMEM-GlutaMAX (GIBCO) supplemented with 10% fetal calf serum, 1mM sodium pyruvate and gentamycin (all Invitrogen). HEK293T human embryonic kidney cells (ATCC) were grown in low glucose (1 g/L) DMEM supplemented with 10% fetal calf serum and 1% penicillin/streptomycin. Phoenix™ Eco (Orbigen, a gift from H. Groenemeyer, IGBMC) human embryonic kidney retrovirus packaging cell line was grown in high glucose DMEM-GlutaMAX supplemented with 10% fetal calf serum and gentamycin. PKD1-PKD3 fl/fl and PKD1/PKD3 DKO MEFs were grown in high glucose DMEM-GlutaMAX supplemented with 10% fetal calf serum, 1mM sodium pyruvate and gentamycin.

METHOD DETAILS

Cell cycle synchronization treatments

Cells were synchronized in different stages of cell cycle by DTBRprotocol. Briefly, 2 mM Thymidine was added twice for 16 hours with three times wash with warm media and Thymidine-free 8 hours incubation in between. After the second Thymidine block was complete, cells were released in thymidine-free media and collected at the indicated time points. Cells were synchronized in G2 using CDK1 inhibitor RO-3306 for 20 hours at 5 μM final concentration. Cells were synchronized in prometaphase using Nocodazole for 8 hours or 14 hours at 3 μM final concentration, Taxol for 16-18 hours at 1 μM, STLC for 18 hours at 5 μM, monastrol for 16 hours at 100 μM. Cells were released from monastrol by washing with pre-warmed DMEM and centrifuged 3 times. Cells were re-plated and were collected in different time points after the release in order to enrich all mitotic phases.

Cell treatments

To activate AMPK, HEK293T WT and AMPK α1/α2 dKO were stimulated for 1 hour with vehicle (DMSO) or 1 μM Rotenone or 10 μM Antimycin or 20 μM CCCP. To inactivate PKD HeLa cells were treated with solvent (PBS) or PKD inhibitor (CRT 0066101, 10 μM) for 1 hour. To inhibit proteasomal degradation cells were treated with solvent (DMSO) or 50 μM MG132 for 2 hours.

Cloning and mutagenesis

Human MFF isoform2 of 291aa, (Q9GZY8, uniprot.org) and MFF isoform4 of 218aa, (Q9GZY8, https://uniprot.org) were amplified from HeLa cDNA by PCR. A single FLAG tag along with KOZAK sequence was inserted in frame at the N terminus of MFF. Human MFF WT and Ser to Ala mutants were cloned into pcDNA3.1/Zeo(+) (Invitrogen) and subcloned into pLenti-CMV-Blast and pGEX6-P1empty vectors using ligation-independent cloning (LIC). Human MFF phosphorylation sites Ser to Ala mutants were generated by PCR using LIC or site-directed mutagenesis (overlap PCR) strategies. Human MFF WT ΔTMD (transmembrane domain deleted) was generated by PCR as described previously (Otera et al., 2010) and cloned into pGEX6P1 empty vector (GE Healthcare Life Sciences) expressing N-terminal fused GST tag followed by the PreScission protease cleavage site.

Plasmid and siRNA transfections

Transient transfections of plasmid DNA in HeLa cells were performed using JetPEI (Polyplus) according to the manufacturer's instructions. Oligofectamine 2000 RNAiMAX (Invitrogen) was used to deliver siRNAs for gene knockdown according to the manufacturer's instructions at a final concentration of 50 nM siRNA. All siRNA oligonucleotides were purchased from Dharmacon.

Cell transfection and virus production

Retroviral infections were performed using Phoenix™ Eco (Orbigen) packaging cell line using JetPEI transfection reagent following the manufacturer instructions. Briefly, retrovirus producer cell line (10 cm dish) was transfected with 15 μg of plasmid pZip-Neo-SV(X) 1. Retrovirus-containing conditioned media was collected after 36 hours and filtered using 0.45 μm Millex-HV Syringe Filters and

used immediately or stored at 4°C for a few days. MEFs were spinfected in fresh media containing 1 μg/ml polybrene and 50% of lentivirus-containing media for 2 hours at room temperature at 500 g and returned to the cell culture incubator.

Lentiviral infections were performed as described previously (Gehart et al., 2012; Zhang et al., 2017). Briefly, HEK293T cells were used as a packaging cell line using JetPEI (Polyplus Transfection). Transfection mixture for 10cm dish contained 12 μg of Lenti-mix plasmids (3 μg pVSVG, 3 μg pMDL and 3 μg pREV) along with 3 μg of plasmid expressing gene of interest (pLKO.1-puro or pLenti-CMV-Blast) (Campeau et al., 2009). {Citation}16h post-transfection media was replaced by fresh one. Virus-containing conditioned media was collected 24h, 36h and 48 h after transfection, sterile-filtered through 0.45 μm Millex-HV Syringe Filters (Millipore) and used immediately or stored at 4°C. MEFs or HeLa cells were spinfected in fresh media containing 1 μg/ml polybrene and 50% of lentivirus-containing media for 2 hours at room temperature at 500 g and returned to the cell culture incubator. After 36 hours the media was changed and infected cells were selected using puromycin at the concentration of 1 μg/ml until there were no cells remaining on the control plate.

FACS analysis

The BD Celesta was used to analyze HeLa cells. For cell cycle analyses cells were harvested by trypsination and fixed by adding 95% cold ethanol dropwise while mixing gently to reach a concentration of 70% ethanol. Cells were fixed overnight at 4°C. The next day cells were centrifuged and resuspended in PBS. For cell cycle analysis cells were incubated with 40 μg/mL RNase A and 15 μg/mL propidium iodide during 30 minutes, followed by analysis. 30.000 events were counted per condition.

WB

Cells were washed with ice-cold PBS on ice and cell lysates for WB were prepared using lysis buffer (50 mM Tris-HCl pH7.5, 150 mM NaCl, 1% Triton X-100, 1 mM EDTA, 1 mM EGTA, 2 mM Sodium pyrophosphate $Na_4P_2O_7$, 1 mM Sodium vanadate $NaVO_4$ and 50 mM Sodium fluoride NaF) supplemented with protease inhibitors (Complete Protease Inhibitor Cocktail, Roche) and incubated on ice for 10 minutes. After centrifugation at 16 000 g for 10 minutes at 4°C cleared supernatant was transferred to the new tubes and was used immediately or flash-frozen in liquid nitrogen and stored at −80°C until used. Total protein was measured using the Bradford method by Bio-Rad Protein Assay kit (Bio-Rad). Samples (50-100 μg of total protein content) were boiled in 1x Laemmli Sample Buffer and resolved on 8%, 10%, 11% or 12% acrylamide gels using standard Tris-Glycine SDS-PAGE. Proteins were transferred to PVDF membranes (Millipore) and blotted with antibodies listed in the Antibodies section. For membrane blocking and primary antibody dilution 5% BSA (v/v) in PBST was used. All incubations with primary antibodies were performed for 16 hours at 4°C. Blots were developed using SuperSignal West Pico (Pierce, Ref. 34580) or Luminata Forte Western HRP substrate (Merck Millipore, Ref. WBLUF0500).

Fractionation

Isolation of mitochondrial and cytoplasmic fractions was carried out as previously described (Wieckowski et al., 2009) with some adaptations. Briefly, cells were homogenized using a 15 mL Dounce tissue grinder in a buffer containing 30 mM Tris-HCl, pH 7.4, 225 mM mannitol, 75 mM sucrose, and 0.05 mM EDTA supplemented with protease inhibitor cocktail. After 150 strokes with a tight pestle, a small fraction of homogenized cells was resolved by SDS-PAGE (whole cell extract) and the rest was centrifuged at 600 g for 5 min to remove nuclei and intact cells. The supernatant was centrifuged at 10,000 g for 10 min to separate the cytoplasmic fraction (supernatant) from the crude mitochondria fraction (pellet). Crude mitochondria pellet was resuspended in ice-cold mitochondria resuspending buffer containing 5 mM HEPES-KOH, pH 7.4, 250 mM mannitol, and 0.05 mM EDTA and resolved by SDS-PAGE.

Immunoprecipitations

Cells were washed with ice-cold PBS on ice and cell lysates for immunoprecipitation were prepared using IP buffer (50 mM Tris-HCl pH7.5, 50 mM NaCl, 0.5% Triton X-100, 0.5% NP40, 5 mM EDTA, 5 mM EGTA, 1 mM Sodium vanadate $NaVO_4$ and 10 mM Sodium fluoride NaF) supplemented with protease inhibitors (Roche) and incubated on ice for 10 minutes. After centrifugation at 16 000 g for 10 minutes at 4°C cleared supernatant was used immediately or flash-frozen in liquid nitrogen and stored at −80°C until used. Lysates were equilibrated to volume and concentration. For Flag-MFF immunoprecipitation, Anti-FLAG M2 Affinity Agarose Gel (Sigma, Ref. A2220) was used. For GFP-PKD or GFP-MFF immunoprecipitation, GFP-Trap-A beads (ChromoTek) were used. Samples were incubated with the beads for 2 or 16 hours at 4°C. The beads were washed four times with IP buffer and then either directly eluted in 1.5x Laemmli Sample Buffer or eluted with FLAG-peptide. Eluted samples were boiled in 1.5x Laemmli Sample Buffer for 5 minutes and resolved by SDS-PAGE gel. Samples were analyzed by WB as described above.

For immunoprecipitation under denaturing conditions, MFF WT and MFF KO HeLa cells were transfected with HA/His Ubiquitin and GFP-CyclinB1 or with HA/His Ubiquitin pEGFP-N1 and synchronized by monastrol for 18 hours. Cells were released in the presence of 50uM MG132 and were lysed in Urea lysis buffer (8M Urea, 300 mM NaCl, 50 mM Na2HPO4, 50 mM Tris-HCl and 1 mM PMSF, pH 8). After sonication supernatants were cleared by centrifugation at 16 000 *g* for 15 minutes and incubated with GFP-Trap agarose beads (Chromotek) overnight at 4°C. Beads were washed by Urea lysis buffer, eluted in 2 × Laemmli buffer and analyzed by WB.

In silico PKD substrate identification

MFF was identified as a potential PKD substrate by phospho-proteomic study in human cells (Franz-Wachtel et al., 2012). In that study, several MFF phosphosites were discovered to be differentially phosphorylated in HEK293T cells upon expression of

constitutively active form of human PKD1, out of which several contained optimal PKD consensus motif (I/L/VXRXXpS/T). Sequence analysis of MFF orthologs in different species revealed high level of conservation of these sites in vertebrates. Further search showed that pS155 and pS172 (both within optimal PKD motifs) were highly enriched in phospho-proteomic studies performed on cancer cells (Britton et al., 2014; Mertins et al., 2016; Yi et al., 2014) and in mitosis (Kettenbach et al., 2011; Olsen et al., 2010).

Recombinant protein expression and purification

Recombinant Arfaptin 1 was purified as described previously (Gehart et al., 2012). MFF proteins were purified as described previously with slight modification (Otera et al., 2010). Briefly, N-terminally GST-tagged human MFF ΔTMD WT and mutant proteins were expressed in protease deficient BL21DE3 *E. coli* strain using pGex-6P1 vectors. Bacteria were grown in 2xLB at 37°C until log phase (OD600 = 0.5). Thereafter cultures were transferred to 20°C incubator and MFF expression was induced by addition of 0.5 mM isopropyl-β-D-thiogalactopyranosid (IPTG) for 16h. Bacteria were pelleted at 5 000 g for 15 minutes. Cell pellets were resuspended in lysis buffer (PBS, 1% Triton X-100, 1% NP40, 1mM DTT, Lysozyme (100 ug/ml) (Sigma, Ref. 62970), protease inhibitors (Roche), incubated on ice for 30 minutes and sonicated. Lysate was cleared by centrifugation at 15 000 g for 30 minutes at 4°C. Obtained supernatant was incubated for 16 h with 500 μl of Glutathione Sepharose 4B (GE Healthcare) protein purification resin (per 500 mL of bacterial culture used) on orbital shaker at 4°C. Beads were washed four times with 10 mL of lysis buffer and resuspended in 1mL of lysis buffer containing 2 units/μl PreScission Protease (GE Healthcare). GST-tag cleavage was performed for 16 h at 4°C and protease was removed by addition of 50 μl of fresh GSH-resin and centrifugation. Obtained supernatant was dialysed, aliquoted and stored at −80°C in PBS containing 2mM DTT, 20% Glycerol and protease inhibitors (Roche).

In vitro kinase assay

Kinase assays were performed as described previously (Gehart et al., 2012; Hausser et al., 2005; Sumara et al., 2009) with minor modifications. Briefly, for non-radioactive kinase assay, 1 μg of recombinant GST-tagged human MFF ΔTMD WT and mutant proteins were incubated with 25 ng of recombinant human PKD1 (Enzo, Ref. BML-SE348-0005) in Kinase Buffer (50mM Tris pH 7.4, 10mM MgCl2 and 2mM DTT). The reaction started with addition of 200 μM cold ATP and maintained at 30°C. After 30 minutes, 2x SDS-sample buffer was added to terminate the assay. Immediately, samples were loaded and resolved on 12% SDS-PAGE gel. Gel was transferred to PVDF membrane (Millipore) and analyzed as described in WB section.

For radioactive kinase assay, all steps were similar but 2 μCi [γ-32P]-ATP was used instead of cold ATP. For PKD inhibition experiment, solvent (PBS) or 1 μM CRT 0066101 was added to kinase reaction. SDS-PAGE gel containing radioactive samples was fixed and stained with Coomassie Brilliant Blue staining solution, followed by four steps in Coomassie Destain solution (water, methanol and acetic acid in a ratio of 50/40/10 (v/v/v)). After destaining gel was dried on a gel vacuum drier and analyzed by autoradiography exposing to Hyperfilm MP (Amersham).

Mass-spectrometry analysis

Mass-spectrometry analysis was performed in a double-blinded manner. Briefly, non-radioactive kinase reactions containing recombinant human MFF with or without recombinant human PKD, were digested with trypsin and analyzed by LC-MS/MS on Oribtrap XL. MaxQuant software (Ver.1.5.2.8) was used to process obtained raw files. Database was searched in MaxQuant using Andromeda peptide search engine against the human Swiss-Prot database. Viewer in MaxQuant was used for visualization of identified hits together with the raw data. Mass spectrometry results were analyzed using Skyline (MacCoss Lab Software).

Cytospin and IF

Cells were collected from dishes with cell scrapers, centrifuged on Thermo Scientific Shandon Cytospin 4 Cytocentrifuge for 5 minutes at 1000 rpm and fixed with 4% PFA for 10 min at room temperature. Cells were rinsed 3 times with PBS and permeabilized with 0.5% NP40 for 5 min, washed with PBS-Triton 0.01% and blocked with 3% BSA for 1h. Cells were subsequently incubated with primary antibodies in blocking buffer for 1h at room temperature, rinsed 3 times with PBS-Triton 0.01% and incubated with secondary antibodies in blocking buffer for 45 min at room temperature in the dark. After incubation, cells were washed 3 times with PBS-Triton 0.01% and glass coverslips were added on cells already mounted with Mowiol containing DAPI (Calbiochem).

Microscopy

Images were taken with a 63x objective using Zeiss epifluorescence microscope or confocal microscopy (Nikon spinning disk). For live-cell microscopy cells were grown on 35 mm glass bottom disk with four compartments and SiR-DNA (Spirochrom) was added 1h before filming. For the experiments described in Figure 1, cells were synchronized with Double Thymidine and Release Protocol and were filmed 8h after release using a 63x water immersion objective for a total time frame of 7h. Images were acquired every 5 min in stacks of 10 μm range (1 μm steps). For the experiments described in Figure 6, cells were synchronized with Taxol for 24h and were filmed for additional 24h using a 63x water immersion objective. Images were acquired every 10 min in stacks of 10 μm range (1 μm steps). All image analysis was performed using ImageJ software.

Cell Counting and Categorization

At least 100 cells were counted per condition and per experiment, and they were analyzed for their mitotic and mitochondrial phenotype in a blinded-manner. The mitotic phenotype was assessed by DAPI staining based on their morphology: Cells were categorized in those that had normal mitotic shape and those that displayed different types of mitotic defects (chromosome misalignments, lagging chromosomes, anaphase/telophase bridges, polylobed/abnormal nuclei). TOM20 or Mitotracker was used as a mitochondrial marker and cells were divided in two categories based on their mitochondrial morphology (fragmented and fused).

ATP measurement

ATP production was measured by a colorimetric method of acquiring the absorbance OD = 570nm using the ATP Assay Kit (Abcam, ab83355) according to the manufacturer's instructions.

Mitochondrial Potential measurement

Mitochondrial Membrane Potential was measured by fluorescence of JC1 (Abcam, ab113850) according to the manufacturer's instructions.

Colony Formation Assay

500 cells were seeded per well in 6-well plates and were cultured for 14 days until colonies were formed. Cells were washed with 1X PBS, fixed with 4% PFA and stained with 0,1% Crystal Violet for 30min. The number of colonies was automatically counted with Fiji software.

QUANTIFICATION AND STATISTICAL ANALYSIS

All experiments were done in a strictly double-blind manner. At least three independent biological replicates were performed for each experiment and image quantifications were carried out in a blinded manner. Curves and graphs were made using GraphPad Prism and Adobe illustrator software. Data was analyzed using two sample two-tailed t test or one-sample two-tailed t test (two-group comparison or folds increase relative to the control, respectively). The data were expressed as mean ± SD and difference was considered as significant, when p values were: $*p < 0.05$, $**p < 0.01$, and $***p < 0.001$.